
# Yarmouk University
# Hijjawi Faculty for Engineering Technology

## Investigation of line-side harmonics produced by three phase controlled rectifier in terms of firing angle variations.

**A Thesis Submitted to**
**The Department of Electrical Power Engineering**

In partial fulfillment of the requirements for the degree of
Master of Science

By:
**Mhamed Nibras Abou Al shamat**
2012979014

Supervisor:
**Prof. Mohammed Bashir Rifai**

August, 2015

# Investigation of line-side harmonics produced by three phase controlled rectifier in terms of firing angle variations.

By

Mhamed Nibras Abou Alshamat

**B.Sc. in Electrical Engineering, DAMASCUS University, Syria, 2011**

A Thesis submitted in partial fulfillment of the requirements for the degree of Master of Science in the Department of Electrical Power Engineering, Yarmouk University, Irbid, Jordan

**APPROVED BY:**

**Prof. Mohammed Bashir Rifai** M.B.Rifai **Chairman**

Professor of Electrical Power Engineering, Yarmouk University

**Dr. Eyad. A. Feilat.** E.A.Feilat **Member**

Associate Professor of Electrical Engineering, University of Jordan

**Dr. Mohammed Awad AlMomani** M.MOMANI **.Member**

Assistant Professor of Electrical Power Engineering, Yarmouk University

**Engineering, Yarmouk University**

**August, 2015**

# Dedication

First of all I would like to acknowledge in this work to Allah who supported me with patience and strength to complete this thesis and with all cherished love and sincere emotion, I dedicate this innovative work to the ones who sacrificed everything in their life for me, to the ones who always inspire and support me to achieve my goals and live strong, to my adored mother and father.

With deepest appreciation for them, I also dedicate this work to my beloved brothers, Firas, Fadi, and Shadi.

Also I would like to show my greatest appreciation to my dearest friend Eng. Al-Motasem Aldaudeyeh for his support and encouragement throughout my study.

# Acknowledgements

In the name of Allah,

I gratefully thank my advisor, Prof. Mohammed Bashir Rifai, for his wise guidance, helpful suggestions, valuable ideas, and persistence to complete this thesis.

I also thank everyone who has helped me to finish this work successfully. I gratefully appreciate all the support from my parents in this crucial achievement of my life.

# Declaration

Plagiarism is the breach of copyright or using another person's work and pretending that is one's own.

I am, Mhamed Nibras Abou Al shamat, recognize what plagiarism is and I hereby declare that this thesis proposal, which is submitted to the department of Electrical Power Engineering at Hijjawi Faculty for Engineering Technology, for partial fulfillment of the requirements for the degree of Master of Science, is my own work. I have not plagiarized from any sources. All references and acknowledgments of sources are given and cited in my proposal. I have used the conventional citation and referencing. Each significant contribution to and quotation in this report from work of other people has been attributed and referenced.

Mhamed Nibras Abou Al shamat

**Table of Contents:** **Page**

**List of Tables:** **Page**

**List of Figures:** **Page**

## LIST OF ABBREVIATIONS

| Abbreviation | Description |
|---|---|
| $IEEE$ | Institute for Electrical and Electronic Engineers |
| $IEC$ | International Electro Technical Commission |
| $THD_i$ | Current Total Harmonic Distortion |
| $THD_v$ | Voltage Total Harmonic Distortion |
| $ASD$ | Adjustable Speed Drive |
| $L_s$ | AC-Line Reactor |
| $L_d$ | DC-Bus Inductance |
| $L_{add}$ | Additional AC-Line Reactor |
| $DC$ | Direct Current |
| $AC$ | Alternative Current |
| $P-Pulse$ | Number of Pulses |
| $PCC$ | Point of Common Coupling |
| $P.U$ | Per Unit |
| $Hz$ | Hertz |
| $TDD$ | Total Demand Distortion |

| | |
|---|---|
| $\boldsymbol{EMC}$ | Electromagnetic Compatibility |
| $\boldsymbol{RMS}$ | Root Mean Square |
| $\mathbf{I_h}$ | The Magnitude of Individual Harmonic Components |
| $\mathbf{I_{sc}}$ | Short-Circuit Current at the PCC |
| $\mathbf{I_L}$ | Fundamental Component of the Maximum Demand Load Current at the PCC |
| $\boldsymbol{I_1}$ | Fundamental Current |
| $\boldsymbol{I_c}$ | Commutation Current |
| $\boldsymbol{I_n}$ | Harmonic Current of nth Order |
| $\boldsymbol{P_1}$ | Initial Power Consumption of the Motor |
| $\boldsymbol{P_2}$ | Final Power Consumption of the Motor |
| $\boldsymbol{n_1}$ | Initial Speed of the Motor |
| $\boldsymbol{n_2}$ | Final Speed of the Motor |
| $\boldsymbol{r_c}$ | Ripple Coefficient |
| $\boldsymbol{emf}$ | Electromotive Force |
| $\boldsymbol{\alpha_c}$ | Critical Firing Angle |
| $\boldsymbol{v_a, v_b, v_c}$ | Phase Voltages |
| $\boldsymbol{i_a, i_b, i_c}$ | Line Currents |

| | |
|---|---|
| $\boldsymbol{HVDC}$ | High Voltage Direct Current |
| $\boldsymbol{u}$ | Commutation Period |
| $\boldsymbol{\beta}$ | Extinction Angle |
| $\boldsymbol{CCM}$ | Continuous Conduction Mode |
| $\boldsymbol{DCM}$ | Discontinuous Conduction Mode |
| $\boldsymbol{V_m}$ | Maximum Output Voltage |
| $\boldsymbol{V_o}$ | The Mean Value of the Output Voltage |
| $\boldsymbol{h}$ | Harmonic Order |

**Abou Alshamat, Mhamed Nibras. Investigation of line-side harmonics produced by three phase controlled rectifier in terms of firing angle variations. Master of Science Thesis, Department of Electrical Power Engineering, Yarmouk University, 2015 (Advisor: Prof M. B. Rifai)**



## Abstract

The problems of harmonics are remarkably apparent at electrical power system equipment. The impact of harmonics on transformers show up as a rise of transformers losses and heating that could shorten their operating life. During resonance, capacitor bank experience high voltage distortion, which could lead to insulation failure due to excessive peak voltage values. Moreover, the current flowing through the capacitor significantly increases due to higher order harmonics of voltage, and this may lead to fuse blowing due to high harmonic current through it.

The 6-pulse rectifier bridges are still the most common front end topology that is used for Adjustable Speed Drives (ASDs) because they have low cost, high efficiency, and good reliability. However, 6-pulse ASD results in harmonic emissions, which requires methods to reduce them.

The conventional way to eliminate harmonic orders is by using passive filters. For example, single-tuned passive filter, $2^{nd}$ order wide band filter, or C-type filters. Many different ways exist to minimize the line-side harmonics for 6-pulse ASD such as changing line reactor $L_s$, phase shifting transformers, or active filters.

In this thesis, calculations of line-side harmonic currents of a DC motor driven by 6-pulse thyristor rectifier bridge are found using MATLAB/SIMULINK software. Both harmonic currents and THDi are calculated. The effect of different firing angles on harmonic current is shown and mitigation options like AC-inductance and DC-inductance in harmonics are illustrated.

Finally, MATLAB/Simulink is used during the study and work analysis. Results show that the load torque percentage plays a significant role in THDi levels. Moreover, in terms of firing angle variations versus different load

percentage, the simulation results show that the amount of current distortion is at its minimum when operating at lower firing angle and higher load percentage. The increase of $L_{add}$ and/or $L_d$ will result in lower THDi levels.

**Key Words:** Controlled 3-phase rectifier bridge, Current Total Harmonic Distortion, Harmonics, AC Line Inductance, DC-Link Inductance.

# CHAPTER ONE:

## Introduction

# Chapter One: Introduction

## 1.1. Background

There is a lot of time spent trying to reduce the energy bill by all organizations. Better saving is achieved when utilizers actually use less energy in the first place. Currently the common approach is to manufacture products that have high efficiency and one example is the concept of ASDs.

ASD effectively allows speed variation of the motor to precisely match a reference speed and in doing so we eliminate the wasted energy that is associated with running motor traditionally at full speed and therefore allows to minimizing energy wastage.

Control techniques of ASDs can help us achieve huge energy savings. For instance, applying ASD to centrifugal fans and pumps offers extremely good energy saving opportunities as high as sixty percent in some applications. The saving potential is high at variable torque applications when using ASD because centrifugal fans and pumps follow what are called the "Affinity Laws" as in [1]. The laws of physics basically state that flow is approximately proportional to speed but the power consumed is roughly proportional to the cube of the speed as follows [1]:

$$\frac{P_1}{P_2} = \left(\frac{n_1}{n_2}\right)^3 \tag{1.1}$$

Where:

$P_1$ Initial power consumption of the motor [watt].

$P_2$ Final power consumption of the motor [watt].

$n_1$ Initial speed of the motor [r.p.m].

$n_2$ Final speed of the motor [r.p.m].

This means that slight speed reduction gives us a big drop-off in power consumption. For example, if the motor speed is reduced by 30%, motor power consumption is reduced by a cubic relationship ($0.7 * 0.7 * 0.7$), or 65.7%.

With the present rapid improvement of power electronics and microprocessors, the use of ASDs is increasing day after day. However, ASDs are considered as one of the main causatives of harmonic distortion in an AC power system [10]. In order to avoid any damage or misoperation of electric equipment, harmonic distortion should be assessed and controlled. As a result of the detrimental effects of harmonics, both electric utilities and end users are becoming more interested in power quality and harmonic mitigation techniques.

## 1.2. Definition of Power Quality

A common power quality problem definition is mentioned in [2], which states that any deviation appears in standard voltage, current, or frequency waveforms that leads to misoperation of utilizer's apparatus. Institute for Electrical and Electronic Engineers (IEEE) has set standards to deal with power quality problems. These standards determine the amount of current and voltage harmonic distortion that is acceptable at the Point of Common Coupling (PCC) [3].

## 1.3. Power quality problems

According to statistics, the most frequent power quality problems are voltage sag, voltage swell, voltage flicker and harmonics [5].

### 1.3.1. Voltage Sag

A voltage sag (or voltage dip) happens when there is a decrease between 0.1 p.u and 0.9 p.u in the nominal voltage at the fundamental frequency for the duration of 0.5 cycle to 1 minute (short duration under-voltage). Voltage sags are mainly caused by adding heavy loads, starting large motors and faults (short circuits) on power systems. Dips may lead to misoperation of sensitive devices as well as failure of digital computers and other power electronic devices [5].

### 1.3.2. Voltage Swell

A voltage swell occurs when there is an increase between 1.1 to 1.8 p.u of the nominal voltage for duration of 0.5 cycle to 1 minute (short duration over-voltage). The main cause of voltage swells are faults on power system and inserting a large capacitor banks [5].

### 1.3.3. Voltage Flicker

A voltage flicker could be depicted by either systematic or random changes in the voltage envelop. In other words, voltage flicker is simply a fluctuation in the voltage waveform that does not usually exceed the voltage ranges of 0.9 p.u to 1.1 p.u. The main reasons for the occurrence of voltage flicker are loads that experience sudden or continuous changes in the load current, for instance, arc furnaces and welding machines [6].

### 1.3.4. Harmonics

Harmonics are currents and voltages with frequencies that are integer multiples of the fundamental frequency 50 or 60 Hz. An introduction to harmonic sources is mentioned in [7]. For example, arcing devices, magnetic circuits, power electronics devices are all sources of harmonics, and the ASDs which will take much of our concern.

The effect of harmonics usually appears first at capacitor banks which may lead to either parallel or series resonance. These results into high current at harmonic frequencies that could cause overheating, high peak voltage and even blowing of the fuses [8]. On the other hand, voltage distortion at the motor terminals due to harmonic distortion appears as harmonic fluxes leading to additional losses, heating and torque pulsating [2]. One other major impact of harmonic distortion can be seen in transformers, and this impact appears in form of extra losses, which are due to $I^2R$ losses, eddy current losses, and stray losses. As a result, these losses can have an enormous influence in lessening the

operating life of a transformer [9]. Moreover, these harmonic currents can lead to interference with telecommunication lines and errors in power metering.

Because of the aforementioned detrimental effects of harmonics, several methods have been followed in order to reduce harmonic current. Some of them are based on raising the ability of electric equipment to withstand harmonic current such as de-rating transformers or increasing the cross section of the neutral conductor as in [10], while others are based on cancelling or mitigating harmonic currents, such as passive tuned filters, multi-pulse rectifiers or active power filters as in [3]. The influence of the electrical environment and power supply on ASD and the procedures and techniques that could be followed to enhance the immunity of ASD against electrical disturbances they are all discussed in [11].

The 6-pulse rectifier bridge is still the most common front end topology that is used for ASDs because they have low cost, high efficiency and good reliability. However, 6-pulse ASD emits large amount of harmonics. The conventional way to eliminate harmonic currents is by using tuned passive filters because they are simple and not expensive. Many other different ways exist to minimize the line-side harmonics for 6-pulse ASD such as changing line reactor $L_{add}$ and/or changing the DC-link inductance $L_d$ [8].

When electric load draws current that is sinusoidal in shape and proportional to the applied sinusoidal voltage, the load is referred to as linear load. On the other hand, if the electric load draws current that is not sinusoidal in shape compared to the applied sinusoidal voltage the load is referred to as non-linear load. In other words, non-linear load draws periodic non-sinusoidal current (distorted current waveform) and that current can be represented by fundamental sinusoidal current in addition to integer multiple of the fundamental (harmonics). Analyzing this distorted current waveform is the process of computing the amplitudes and the phases of the fundamental and higher order harmonic of the periodic waveform that is done by means of Fourier series concept.

In certain circumstances linear loads such as motors generators and transformers produce comparatively small amount of harmonics compared to non-linear loads. For instance, due to unequal distribution of windings in rotating machines the magneto-motive force is unequally distributed and that causes

harmonic production. In transformers, as a result of non-linear characteristics of magnetic material above the knee point, current and voltage are not sinusoidal and include harmonic.

## 1.4. Power quality standards

### 1.4.1. IEEE 519-1992 Standard

To reduce any possible damage that may result from harmonic distortion, IEEE Standard 519-1992 recommends the amount of current and voltage harmonic distortion that is acceptable at the Point of Common Coupling (PCC) [3]. Recommended limits are provided for both individual harmonic components and the Total Demand Distortion (TDD). The TDD refers to the ratio between the RMS value of current harmonics of order higher than two and the maximum demand load current $I_L$ at fundamental frequency taken at the PCC.

$$TDD = \frac{\sqrt{\sum_{h=2}^{h\_max} I_h^2}}{I_L} \times 100\% = \frac{\sqrt{(I_2^2 + I_3^2 + \cdots I_{hmax}^2)}}{I_L} \times 100\% \quad (1.2)$$

Where :

$I_h$ The magnitude of individual harmonic components [A].

$I_{sc}$ The short-circuit current at the PCC [A].

$I_L$ The fundamental component of the maximum demand load current at the PCC [A].

Table 1.1 shows current limits for individual harmonic components as well as total harmonic distortion.

**Table 1.1** Current Distortion Limits for Distribution Systems at PCC (120 V-69,000 V) [3].

| $I_{sc}/I_L$ | $\leq 11$ | $11-17$ | $17-23$ | $23 \leq h < 35$ | $35 \leq h$ | TDD |
|---|---|---|---|---|---|---|
| $< 20$ % | 4 | 2 | 1.5 | 0.6 | 0.3 | 5 |
| $20-50$ % | 7 | 3.5 | 2.5 | 1 | 0.5 | 8 |
| $50-100$ % | 10 | 4.5 | 4 | 1.5 | 0.7 | 12 |
| $100-1000$ % | 12 | 5.5 | 5 | 2 | 1 | 15 |
| $> 1000$ % | 15 | 7 | 6 | 2.5 | 1.4 | 20 |

Table 1.2 shows voltage limits for individual harmonic components as well as total harmonic distortion.

**Table 1.2** Voltage Distortion Limits [3].

| Bus voltage at PPC | Individual Voltage Distortion (%) | Total Voltage Distortion THD (%) |
|---|---|---|
| **69 KV and below** | 3.0 | 5.0 |
| **69 KV -161 KV** | 1.5 | 2.5 |
| **161KV and above** | 1.0 | 1.5 |

Voltage total harmonic distortion can be calculated as in equation (1.3):

$$THD_v = \frac{\sqrt{\sum_{h=2}^{h\_max} v_h^2}}{v_1} \times 100\% = \frac{\sqrt{(v_2^2 + v_3^2 + \cdots v_{hmax}^2)}}{v_1} \times 100\% \qquad (1.3)$$

Where :

$v_1$ Fundamental voltage.

$v_h$ Harmonic voltage of nth order.

### 1.4.2. IEC 61000 EMC

The fundamental disagreement when comparing IEEE standards and IEC 61000 is that IEEE-519 standards define the limits of the harmonic currents generated by non-linear loads and injected into the electric grid as well as the limits of the harmonic voltages at the grid buses, whereas the purpose of Electromagnetic Compatibility (EMC) Standards from IEC 61000 is to decrease the harmonic participation of electric apparatus [4].

IEC provide various standards that decrease harmonic participation [4]:

- **IEC 61000-3-2:** Limits for harmonic current emissions for load currents up to 16 A.
- **IEC 61000-3-3:** Limits for voltage distortion in low-voltage power supply systems for equipment with rated current ≤ 16 A.
- **IEC 61000-3-4:** Limits for harmonic current emissions for load currents higher than 16 A (Table 1.3).
- **IEC 61000-3-5:** Limits for voltage distortion in low-voltage power supply system for equipment with rated current > 16 A.

**Table 1.3** Harmonic emission limits: IEC 61000-3-4 [4].

| Harmonic number n | Maximum harmonic current $\frac{I_n}{I_1}\%$ |
|---|---|
| 3 | 21.6 |
| 5 | 10.7 |
| 7 | 7.2 |
| 9 | 3.8 |
| 11 | 3.1 |
| 13 | 2 |
| 15 | 0.7 |
| 17 | 1.2 |
| 19 | 1.1 |
| 21 | $\leq 0.6$ |
| 23 | 0.9 |
| 25 | 0.8 |
| 27 | $\leq 0.6$ |
| 29 | 0.7 |
| 31 | 0.7 |
| 33 | $\leq 0.6$ |
| Even | $\leq 8/n$ or $\leq 0.6$ |



Where:

$I_1$ Rated fundamental current.

$I_n$ Harmonic current of nth order.

## 1.5. Harmonic Mitigation Using Filters

### 1.5.1 Types of filters

Passive filtering techniques are one of the most used approaches for control of harmonic distortion in the power system. A capacitor can be shunt-connected and offers small impedance for harmonics components above specific frequency. Likewise, an inductor can be series-connected and offers a high impedance path for harmonics components above specific frequency. Since filters allow only components of certain frequency to pass, they are called harmonics traps. More complex characteristics of a filter can be obtained by connecting a network of two or more of capacitors, resistors, and inductors. Passive filter can be either tuned to cancel a certain harmonic order or to cancel harmonics over a certain frequency bandwidth [32].

More advanced methods have been investigated to control harmonic levels in the power system. For instance, active harmonic filters (AHF) which are basically power electronic converters that can act as either controlled current source (Shunt Active Power Filter) or controlled voltage source (Series Harmonic Filter). AHFs are smaller by size and lighter by weight compared to large size passive filters. Additionally, active filters have the advantage of eliminating various harmonic orders at a time, whereas passive filters are basically designed to eliminate only one harmonic order [35].

#### 1.5.1.1 Passive Filters

##### 1.5.1.1.1 Series Passive Filter

A series passive filter is connected in series with the load and it consists of inductance and capacitance which are connected in parallel [31]. Series filter is tuned at a certain frequency to provide large impedance and this large impedance stops the harmonic current from flowing within the system at that frequency only. However, the drawback of this arrangement is that the series filter should be designed to carry the full load current. Moreover, it must be equipped with overcurrent protection scheme and as a result extra cost [32].

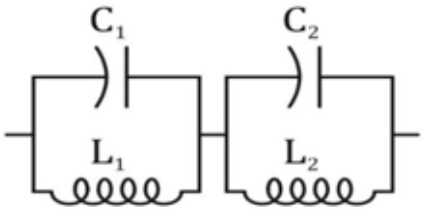


**Fig. 1.1** Series passive filter.

#### 1.5.1.1.2 Shunt Passive Filter

##### 1.5.1.1.2.1 Single Tuned Filter

The topology of the single tuned filter is shown in Fig. 1.2. Single tuned filter is characterized by its low cost and simplicity because it is only a combination of a capacitor C and an inductance L [31]. Moreover, it tends to correct the load power factor as well as remove the harmonic current. However, tuned filter can be tuned to cancel only one harmonic order at a time. As a result we have to use several filters to eliminate unwanted harmonic orders that are present in power system [32].

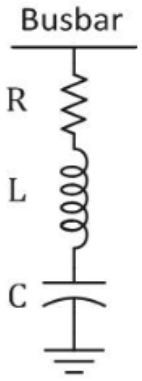


**Fig. 1.2** Single-tuned filter topology

Single tuned filter (also called notch filter) is connected in parallel with the load and it is series-tuned to provide a low impedance branch to the harmonics at a certain frequency to be filtered, that is why sometimes they are called harmonic traps. The values of L and C are chosen so that the tuning frequency of the circuit matches with the harmonic frequency to be eliminated. Generally, the impedance

$Z_f(h)$ of the notch filter branch with respect to harmonic order h can be expressed as [31] as in equation (1.4):

$$Z_f(h) = j\,(h\,X_L - \frac{X_C}{h}) \tag{1.4}$$

The resonance or tuning frequency of this filter can be expressed as [32] as in equation (1.5):

$$f_c = \frac{1}{2\,\pi\,\sqrt{L_f\,C_f}} \tag{1.5}$$

$f_c$ Resonant or tuning frequency in hertz.

$L_f$ Filter inductance in henrys.

$C_f$ Filter capacitance in farads.

$h$ Harmonic order.

The quality factor $Q$ determines the bandwidth and the filtering deepness at the notch frequency which can be given as [32] as in equation (1.6):

$$Q = \frac{\sqrt{\frac{L}{C}}}{R} \tag{1.6}$$

#### 1.5.1.1.2.2 Second Order High-Pass Filter

The topology of the second order high-pass filter is shown in Fig. 1.3. This type of filters is used to mitigate multiple high order harmonics, and it is also characterized by its shallow notch when comparing to single tuned filter due to high impedance value at the same harmonic order [31]. As a result, it is not as sensitive as the single tuned filter to parameter changes. Another advantage is the acceptable amount of losses at fundamental frequency compared to other frequency. Due to previous advantages, second-order high-pass filters are widely used for different industrial applications like high power adjustable speed drives (ASDs) [32].

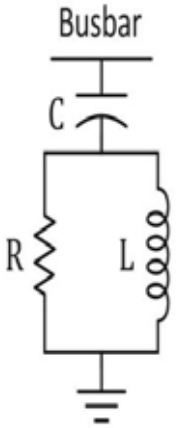


**Fig. 1.3** Second-order high-pass filter topology.

Generally, the impedance $Z_f(h)$ of the second-order high-pass filter branch with respect to harmonic order h can be expressed as [31] as in equation (1.7):

$$Z_f(h) = \frac{R\,(h\,X_L)^2}{R^2 + (h\,X_L)^2} + j\,(\frac{R^2 h\,X_L}{R^2 + (hX_L)^2} - \frac{X_C}{h}) \tag{1.7}$$

### 1.5.1.1.2.3 C-Type Filter

The topology of the c-type filter is shown in Fig. 1.4. Compared to other type high-order filters, this type have a moderate performance and it is used to eliminate lower order harmonics than the other high-pass filters [31]. Moreover, these sorts of filters face no losses at the fundamental frequency; that is, due to the extra capacitor C2 which is added in series with the inductor L and they are tuned at the fundamental frequency. However, it is less efficient in mitigating high order harmonics than the second-order high-pass filter [32].

Generally, the impedance $Z_f(h)$ of the C-type filter branch with respect to harmonic order h can be expressed as [32] as in equation (1.8):

$$Z_f(h) = \frac{R\left(h\,X_L - \frac{X_L}{h}\right)^2}{R^2 + \left(h\,X_L - \frac{X_L}{h}\right)^2} + j(\frac{R^2\left(h\,X_L - \frac{X_L}{h}\right)}{R^2 + \left(h\,X_L - \frac{X_L}{h}\right)^2} - \frac{X_C}{h}) \tag{1.8}$$

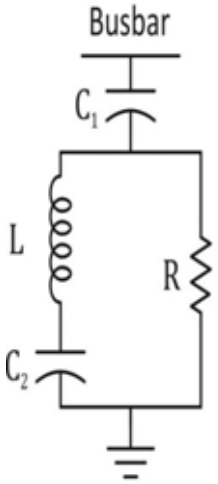


**Fig. 1.4** C-type high-pass filter topology.

### 1.5.1.2 Active Harmonic Filter (AHF)

#### 1.5.1.2.1 Shunt Active Harmonic Filter

Shunt active power filters (SAHFs) are basically power electronic converters applied as controlled current source [33]. They are connected in parallel with the power system as close as possible to the non-linear load to prevent the circulation of harmonics to the reminder of the electric grid. SAHF injects currents equal in magnitude to the harmonic currents produced by the non-linear load, however, shifted by 180. These currents cancel out harmonics currents produced by that load. SAHFs are characterized by small size and low weight compared to large size passive filters. Additionally, active filters have the advantage of eliminating various harmonic orders at a time, whereas passive filters are basically designed to eliminate only one harmonic order [34].

#### 1.5.1.2.2 Series Active Filter

Series active filters (SAFs) are basically power electronic converters applied as controlled voltage source [33]. SAFs are placed in series with the electric grid and near the non-linear load. The voltage produced by the filter with a desired frequency stops the harmonic current with the same frequency from circulating back to the source. That is because SAF presents high impedance when boosting the voltage produced by the filter. The disadvantage of this configuration is the

extra cost accompanying with the transformer that links the SAF to the grid to allow the filter to insert the required voltage [34].

It can be concluded that active filters have the advantage of eliminating various harmonic orders at a time, whereas passive filters are basically designed to eliminate only one harmonic order. Although active filters offer wide range of harmonic cancellation and characterized by their small size and light weight compared to passive filters, however, they are much more complicated and expensive since they require control circuit and many other components. Thus, passive filters still the favorable choice when talking about harmonic cancellation technique. The next chapter illustrates the circuit diagram, analytical relations and waveforms of output voltage and current of a single-phase controlled bridge rectifier supplying different types of loads.

## 1.6. Motivation

Since ASDs are increasingly used in industry, more harmonics will be injected due to their presence. Thus, it is important to consider further investigations about how harmonics magnitudes vary depending on circuit topology, parameters, and operating conditions. Previous researches addressed harmonics assuming idealized conditions like smooth DC current (that is, very large $L_{dc}$) and pure mains supply (no equivalent inductance of the source), and RL load rather than actual DC motor [18]. This thesis examines the harmonics injection of ASDs (to the grid) with more practical assumptions which helps to verify validity of the idealized conditions.

## 1.7. Contribution

This thesis examines the effect of more practical parameters and operating conditions of DC drives. Specifically, it accounts for the effect of source inductance $L_s$, DC-link inductance $L_d$, and actual DC motor load rather than ideal conditions. Firing angle variation will be considered and its effects on THDi injection will be addressed. In addition, the impact of load alteration in terms of firing angle variation on THDi will be presented in this thesis.

## 1.8. Thesis Objective

The main objective of this thesis is to conduct a model consisting of a 6-pulse controlled rectifier bridge driving a DC motor using MATLAB/SIMULINK software, and then to study the influence of firing angle variations on harmonic currents and THDi at the AC line-side. Next, the roles that source inductance $L_s$ and DC-link inductance $L_d$ play in harmonic mitigation are illustrated.

## 1.9. Scope of Thesis

Scope of thesis can be executed through the following steps:

1. Studying six-pulse rectifiers and ASDs, their operation, and their harmonics contents.
2. Modelling six-pulse rectifier in Simulink considering practical parameters.
3. Simulating the harmonics injection into the grid with different firing angles.
4. Inserting different inductance values for both AC side and DC side to the model and study there effect on harmonic currents.
5. Verifying results and drawing conclusions based on them.

## 1.10. Thesis Organization

The thesis is organized as follows:

Chapter 1 introduces the power quality problems in the power system, the effect of harmonics on different electric equipment and illustrates power quality standards. Chapter 2 presents the literature review on the applications that are used to estimate and mitigate harmonics in the power system. Chapter 3 illustrates the analytical expressions of multi-pulse rectifier bridges. Moreover, it shows their reduction effect over total harmonic distortion. In chapter 4 the results and simulation are given. Chapter 5 presents the conclusion of this thesis and suggestions for future work.

# CHAPTER TWO:

## Literature Review

# Chapter Two: Literature Review

## 2.1. Literature Review

Authors of [12] mainly discuss four level of modeling the single-phase diode rectifier starting with ideal model which has a very limited accuracy but nearly no parameters are needed, ending with numerical model which has high accuracy however, too many parameters are needed. Furthermore, measurements of real application are compared with these models and the results validated the suggested method.

In reference [13] table-based model for a 6-pulse uncontrolled rectifier was used to calculate line side-harmonics, a look-up table of the current total harmonic distortion THDi was established depending on multiple simulations, independently either one of the system parameters is changed. Results show a very high harmonic content when both AC and DC inductances have small values and a continuously decreasing harmonic content as these inductances will have bigger values. The proposed method was compared to a real application and the results were quite accurate regarding the harmonic current estimation.

Authors of [14] propose a combination of empirical method and analytical expressions for estimation of line side harmonic currents of diode rectifier when connecting with multiple-pulse diode rectifier. This is done by "splitting" the original diagram into multiple ones and each three-phase rectifier bridge is analyzed separately using circuit simulator. Ultimately, a correction factor (compensation factor) due to mutual impact between parallel three-phase rectifier bridges is applied to re-combine the original diagram. Outcomes of this technique were compared with real application measurements and they showed a good match. As a result, less time and little calculation are achieved.

In paper [15], in addition to DIgSILENT, Pspice, new harmonic calculation software is presented in order to accomplish harmonic estimation for a large ASD. The new software MCT31 is done using a combination of pre-collected database and interpolation techniques. Harmonic simulation results of

three software are compared with results taken from real application. The new software shows efficient results even with limited data-input.

Authors of [16] provide a new approach to calculate harmonic currents produced by 12-pulse and 18-pulse drives. This is done by developing harmonic calculation toolbox devoted specifically for harmonic analysis on 6-pulse drives. As a result, a simple and speedy software operation can be achieved. It also illustrates comparison results of different simulation results to reduce line harmonic currents, these topologies are developed for 6-pulse rectifier bridge with a chance to add AC-inductance $L_{add}$or DC-inductance $L_d$, and were also used for 12-pulse and 18-pulse.

For a three-phase controlled rectifier with RL-load reference [17] provides a delicate statistical solution based on MATLAB Simulation to find current harmonics and THD for different firing angles.

In [18], assuming the inductance of DC-link $L_d$ is too large and the inductance of the Ac-side $L_s$ equal to zero the authors derived the ideal form of the harmonics of the line-side current of a 6-pulse Ac to DC converter.

The concept of active compensation was firstly introduced in 1958 when authors of [21] suggested using a feedback amplifier technique to compensate for voltage harmonics produced by saturated ferromagnetic materials.

In [22] a new method was proposed to cancel out current harmonics in HVDC transmission system. Authors' method was relied on the precept of magnetic flux compensation in a transformer core. That is done by means of compensating currents that are injected into a tertiary winding.

In [31], a comprehensive design study of passive filters is done. The study shows that for high power industrial application, passive filters are widely used due to their reasonable price and good performance. Moreover, it shows the significant effect of the system impedance on the filter. Additionally, it illustrates that the sharpness of the tuning depends on the resistance and the reactor of the filter at the tuned frequency.

In [32], single and double tuned passive filters are proposed to reduce harmonic currents. Results show that for better harmonic cancelation, filters are

placed closer to loads that produce harmonic currents. Moreover, lower THD can be achieved when removing the power factor correction capacitor. Additionally, THD is slightly higher when loads are decreased.

In [33], authors propose to use active power filter (APF) in order to reduce harmonic distortion, this method is based on power electronics technique and offer harmonic cancelation for several order harmonic components at a time as well as reactive power compensation. Both voltage and current waveforms and THD are shown to be improved in the proposed method.

Authors of [34] suggest simple and cost effective shunt active power filter consists of two pulse-width modulated voltage source inverters, one of them operates at low switching frequency which is connected near the harmonic source (non-linear load) and compensate for current harmonic at low frequencies, whereas, the other one operates at high switching frequency and responsible for compensating current harmonic at high frequencies.

Mainly, four methods are available to investigate the line-side harmonic currents of a 6-pulse controlled rectifier bridge. However, three out of four include, very limited accuracy (ideal model), mathematical complexity (Analytical Model) and larger number of parameters must be known when doing the analysis (numerical based circuit model). On the other hand, the table based model offers fairly good results and accuracy, and only limited numbers of parameters are needed when doing the simulation. Thus, the table based model which has been presented in [12] is chosen to be used in this thesis. The next chapter discusses various techniques for harmonic mitigation, starting with the most common and non-expensive approach which is passive filter ending with more sophisticated one which is active power filter.

# CHAPTER THREE:

## Multi-Pulse Bridges Rectifier

# Chapter Three: Multi-Pulse Bridge Rectifier

## 3.1. Three-phase 6-pulse Bridge Rectifier

A widespread example of ASD is the 6-pulse rectifier bridge (Fig. 3.1). An idealized 6-pulse rectifier bridge. The line inductance $L_s$ is zero and the DC bus inductance $L_d = \infty$ making the output DC current constant. Fig. 3.2 shows model waveforms of the rectifier bridge, where $v_a, v_b$ and $v_c$ are the phase voltages of the supply. $i_{g1}$ to $i_{g6}$ are the gate current pulses for thyristors $T_1$ to $T_6$ respectively and $\alpha$ is the firing angle of the thyristors.

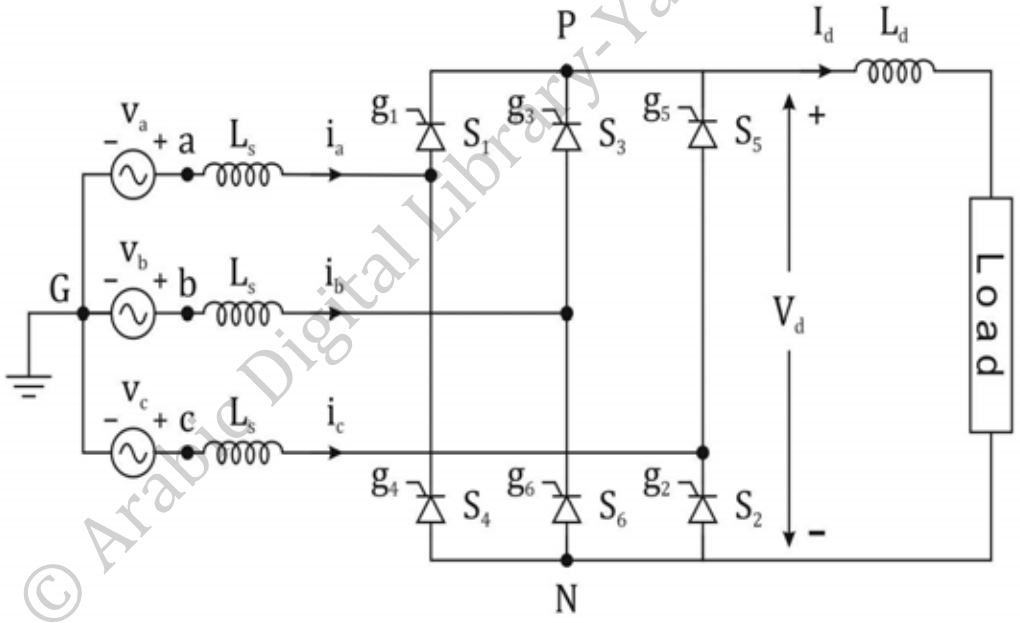


**Fig. 3.1** Simplified circuit diagram of a six-pulse thyristor rectifier.

The phase voltage $v_a$ has the highest value compared to other two phase voltages $v_b$and $v_c$ during period $I$ ($\frac{\pi}{6} + \alpha \leq wt \leq \frac{\pi}{2} + \alpha$), that makes $S_1$forword-baised. However, to turn $S_1$ on a firing pulse is applied to its gate (gate signal $i_{g1}$) at $wt = \frac{\pi}{6} + \alpha$, supposing $S_6$ is turned on before $S_1$ then the resultant positive DC bus voltage $v_p$ with respect to the ground $G$ equal to $v_a$ and the negative DC voltage $v_n$ equal to $v_b$. As a result, the output DC voltage will be equal to

$v_d = v_p - v_n = v_a - v_b = v_{ab}$ and the three phase line currents are $i_a = I_d, i_b = -I_d$ and $i_c = 0$ as illustrated in Fig. 3.2.

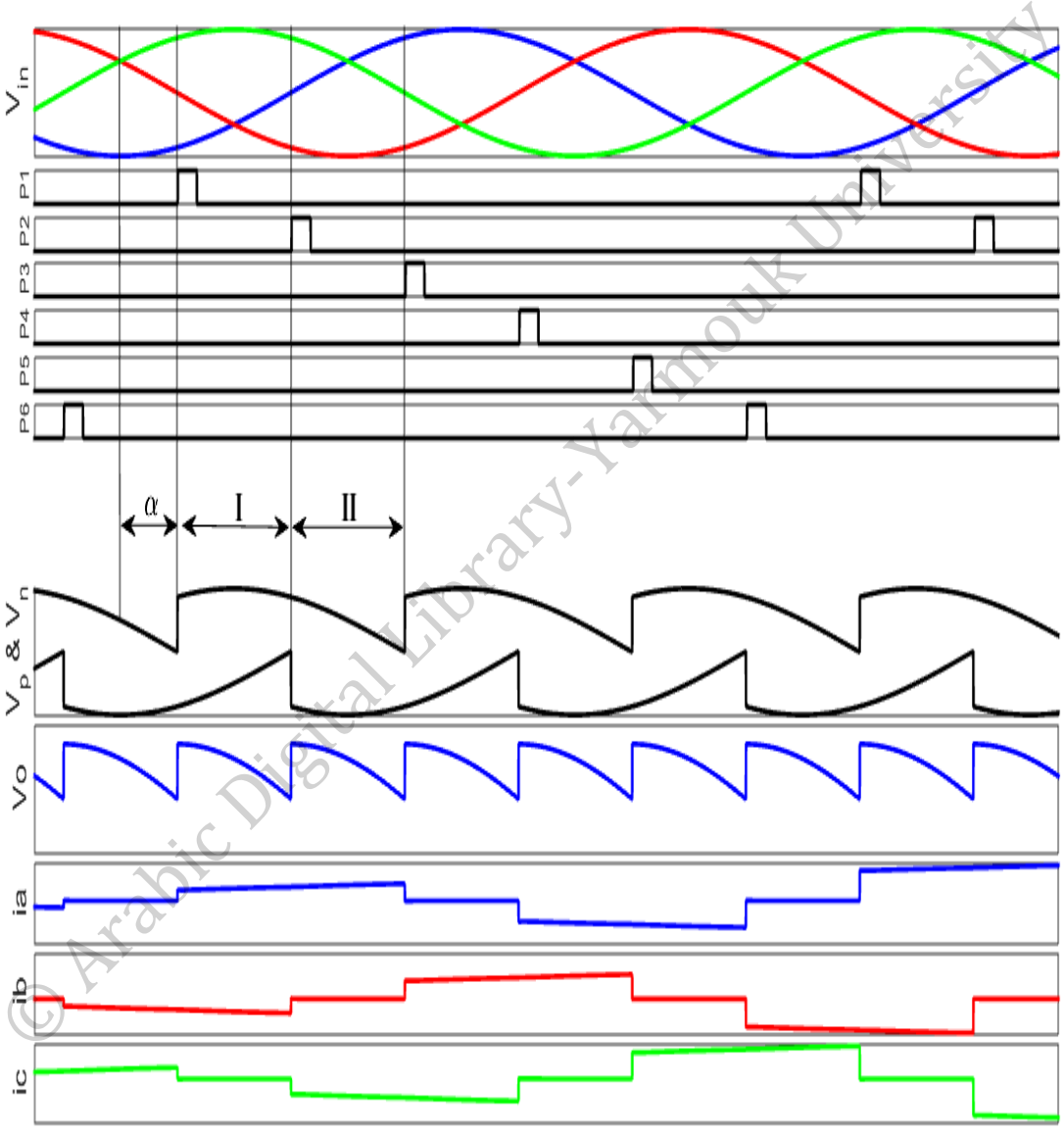




**Fig. 3.2** Waveforms of the idealized six-pulse thyristor rectifier operating at $\alpha = 30°$.

The phase voltage $v_c$ during period II ($\frac{\pi}{2} + \alpha \leq wt \leq \frac{5\pi}{6}$) has the lowest value compared to $v_a$ and $v_b$ that makes $S_2$ forward-biased. However, to turn $S_2$ on a firing pulse is applied to its gate (gate signal $i_{g2}$) at $wt = \frac{\pi}{2} + \alpha$. The turn on of $S_2$ will force $S_6$ to turn off and at that moment of time the DC current $I_d$ is

commutated from $S_6$ to $S_2$ instantly due to the absence of the line inductance. The positive DC bus voltage $v_p$ is still equal to $v_a$. However, the negative DC voltage $v_n$ is equal to $v_c$. As a result, the output DC voltage will be $v_d = v_p - v_n = v_a - v_c = v_{ac}$ and the three phase line currents are $i_a = I_d$, $i_b = 0$ and $i_c = -I_d$.

Following the same process will give us the voltage and current waveforms and expressions of other periods as in [26].

The average DC output voltage can be calculated as in equation (3.1):

$$V_d = \frac{area\ A_1}{\frac{\pi}{3}} = \frac{1}{\frac{\pi}{3}} \int_{\frac{\pi}{6}+\alpha}^{\frac{\pi}{2}+\alpha} v_{ab}\, d(\omega t) = \frac{3\sqrt{2}}{\pi} V_{LL} \cos\alpha = 1.35\, V_{LL} \cos\alpha \qquad (3.1)$$

The line current $i_a$ in Fig. 3.2 can be expressed in a Fourier series as in equation (3.2):

$$\begin{aligned} i_a = \frac{2\sqrt{3}}{\pi} I_d \Big(&sin(\omega t - \emptyset_1) - \frac{1}{5} sin5(\omega t - \emptyset_1) - \frac{1}{7} sin7(\omega t - \emptyset_1) \\ &+ \frac{1}{11} sin11(\omega t - \emptyset_1) + \frac{1}{13} sin13(\omega t - \emptyset_1) \\ &- \frac{1}{17} sin17(\omega t - \emptyset_1) - \frac{1}{19} sin19(\omega t - \emptyset_1) + \cdots \Big) \end{aligned} \qquad (3.2)$$

Where:

$\emptyset_1$ Phase angle between the supply voltage and the fundamental frequency line current $i_{a1}$.

$\omega$ Angular speed.

The rms value of $i_a$ can be calculated as in equation (3.3):

$$I_a = \sqrt{\frac{1}{2\pi} \int_0^{2\pi} (i_a)^2 d(\omega t)} = \sqrt{\left(\frac{1}{2\pi}\right)} \sqrt{\left( \int_{\frac{\pi}{6}+\alpha}^{\frac{5\pi}{6}+\alpha} (I_d)^2 d(\omega t) + \int_{\frac{7\pi}{6}+\alpha}^{\frac{11\pi}{6}+\alpha} (-I_d)^2 d(\omega t) \right)}$$

$$= \sqrt{\frac{2}{3}} I_d = 0.816\, I_d \qquad (3.3)$$

Analytically, the total harmonic distortion THD for the line side current can be calculated as in equation (3.4):

$$THD = \frac{\sqrt{I_a^2 - I_{a1}^2}}{I_{a1}} = \frac{\sqrt{(0.816I_d)^2 - (0.78I_d)^2}}{0.78I_d} = 31\ \% \qquad (3.4)$$

Theoretically, the 6-pulse rectifier bridge is characterized by certain harmonic magnitudes of orders h [2] where $h = 6n \pm 1$ , where n is a positive integer ($n = 1, 2, 3$ ...). Therefore, harmonic orders that would show up in 6-pulse rectifier are $5th, 7th, 11th, 13th, 17th, 19th$, etc. The magnitude of each harmonic is given by $\frac{1}{h}$ p.u. Consequently, the fifth harmonic current constitutes $20\%$ of the fundamental current ($\frac{1}{h} = \frac{1}{5} = 20\%$), the seventh harmonic current constitutes $14.2\%$ of the fundamental current and so on. Theoretically, the total harmonic distortion THD of the idealized 6-pulse rectifier is given as in equation (3.5):

$$THD = \sqrt{I_5^2 + I_7^2 + I_{11}^2 + I_{13}^2 + I_{17}^2 + I_{19}^2 + \cdots} \qquad (3.5)$$

$$THD = \sqrt{20^2 + 14.29^2 + 9.09^2 + 7.69^2 + 5.88^2 + 5.26^2 \ldots}$$

$$THD = 28.43\ \%$$

In either case, theoretically and analytically, the total harmonic distortion $THD$ generated by a there phase idealized 6-pulse bridge which are 28.43 % and 31 % respectively do not satisfy IEEE standards [3]. Thus, higher pulses number should be examined.

## 3.2. P-Pulse Bridge Rectifier

Harmonics accompanying with the 6-pulse rectifiers ($5^{th}, 7^{th}, 11^{th}, 13^{th}, 17^{th}, 19^{th}, \ldots$) have adversely affected the power quality. Consequently, various methods have been implemented to decrease harmonic

emission from ASDs. One popular approach is the use of multi-pulse rectifier bridges with number of pulses bigger than six (12-pulse, 18-pulse, 24-pulse and so on) together with phase shifted secondary transformers. This combination has the advantage of reducing sufficiently lower order harmonic currents produced by 6-pulse rectifier bridge, additionally, it usually does not need LC filter thus, excluding the possibility for LC resonance. As a result of the prior advantages multi-pulse rectifier bridge has become the preferable choice when talking about harmonic mitigation.

### 3.2.1 Three-phase 12-pulse Bridge Rectifier

Fig. 3.3 shows an idealized 12-pulse rectifier bridge consists of two identical 6-pulse bridges. The line inductance $L_s$ as well as the leakage inductance $L_{lk}$ of the transformer and the firing angle $\alpha$ are assumed to be zero. Moreover, the DC bus inductance is assumed to have infinite value ($L_d = \infty$) making the output DC current constant. The two bridges are connected to the same wye primary winding while the other side of transformer is divided into secondary winding with delta connection and tertiary winding with wye connection. As a result of this configuration, 30 degree phase shift angle between the secondary and the tertiary winding currents can be obtained. This type of configuration results in elimination of harmonic current of order 5th, 7th, 17th and 19th. Consequently, the resultant THD would be around 10-12 % compared to 31 % for a single 6-pulse Rectifier Bridge.

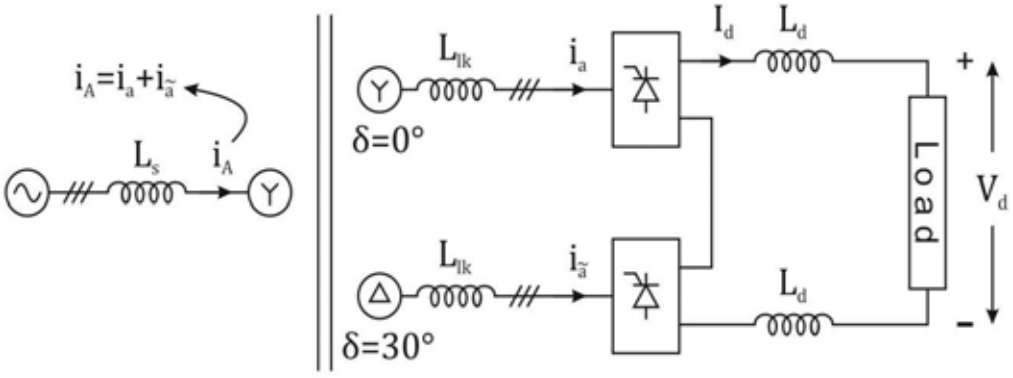


**Fig. 3.3** Simplified circuit diagram of a 12-pulse thyristor rectifier.

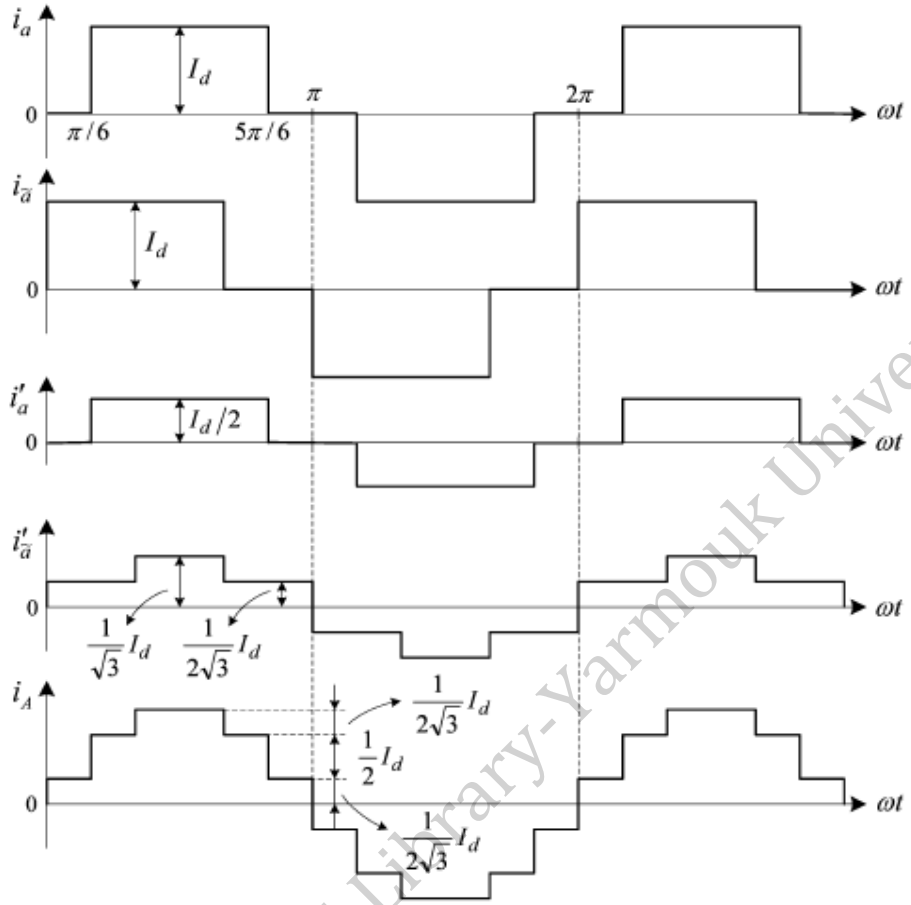


**Fig. 3.4** Current waveforms of a 12-pulse thyristor rectifier [27].

Fig. 3.4 shows the current waveforms for the rectifier, where $i_A$ the primary line current is calculated as in [27] as is equation (3.6):

$$i_A = i'_a + i'_{\tilde{a}} \tag{3.6}$$

$i_a, i_{\tilde{a}}$ Secondary line currents.

$i'_a, i'_{\tilde{a}}$ Primary currents referred from the secondary side.

The secondary line current $i_a$ in Fig. 3.4 can be expressed in a Fourier series as in equation (3.7):

$$i_a = \frac{2\sqrt{3}}{\pi} I_d\left(sin(\omega t) - \frac{1}{5}sin5(\omega t) - \frac{1}{7}sin7(wt) + \frac{1}{11}sin11(\omega t) + \frac{1}{13}sin13(\omega t) - \frac{1}{17}sin17(\omega t) - \frac{1}{19}sin19(\omega t) + \cdots\right) \tag{3.7}$$

The other secondary line current $i_{\tilde{a}}$ in Fig. 3.4 which leads $i_a$ by 30° can be expressed in a Fourier series as in equation (3.8):

$$i_{\tilde{a}} = \frac{2\sqrt{3}}{\pi} I_d(sin(\omega t + 30°) - \frac{1}{5}sin5(\omega t + 30°) - \frac{1}{7}sin7(\omega t + 30°) + \frac{1}{11}sin11(\omega t + 30°) + \frac{1}{13}sin13(\omega t + 30°) - \frac{1}{17}sin17(\omega t + 30°) - \frac{1}{19}sin19(\omega t + 30°) + \cdots) \quad (3.8)$$

When referring the current $i_a$ to the primary side then the resultant current $i'_a$ has similar waveform. However, because of the turns ratio of the Y/Y connected transformer. $i'_a$ has half the magnitude of $i_a$. The line current $i'_a$ can be expressed in a Fourier series as in equation (3.9):

$$i'_a = \frac{\sqrt{3}}{\pi} I_d(sin(\omega t) - \frac{1}{5}sin5(\omega t) - \frac{1}{7}sin7(\omega t) + \frac{1}{11}sin11(\omega t) + \frac{1}{13}sin13(\omega t) - \frac{1}{17}sin17(\omega t) - \frac{1}{19}sin19(\omega t) + \cdots) \quad (3.9)$$

When referring $i_{\tilde{a}}$ to the primary side and due to the Y/Δ connected transformer, the phase angles of harmonic currents are altered. Then the line current $i'_{\tilde{a}}$ can be expressed in a Fourier series as in equation (3.10):

$$i'_{\tilde{a}} = \frac{\sqrt{3}}{\pi} I_d(sin(\omega t) + \frac{1}{5}sin5(\omega t) + \frac{1}{7}sin7(\omega t) + \frac{1}{11}sin11(\omega t) + \frac{1}{13}sin13(\omega t) + \frac{1}{17}sin17(\omega t) + \frac{1}{19}sin19(\omega t) + \cdots) \quad (3.10)$$

The line current $i_A$ can be expressed as in equation (3.11):

$$i_A = i'_a + i'_{\tilde{a}} = \frac{2\sqrt{3}}{\pi} I_d(sin(\omega t) + \frac{1}{11}sin11(\omega t) + \frac{1}{13}sin13(\omega t) + \frac{1}{23}sin\,23(\omega t) + \frac{1}{25}sin25(\omega t) + \cdots) \quad (3.11)$$

The THD of the primary current $i_A$ can be determined by equation (3.12):

$$THD_{i_A} = \frac{\sqrt{I_A^2 - I_{A1}^2}}{I_{A1}} = \frac{\sqrt{I_{A11}^2 + I_{A13}^2 + I_{A23}^2 + I_{A25}^2 + \cdots}}{I_{A1}} = 15.3\ \% \quad (3.12)$$

### 3.2.2 Three-phase 18-pulse Bridge Rectifier

Fig 3.5 shows an idealized 18-pulse rectifier bridge consists of three identical 6-pulse bridges. The line inductance $L_s$ as well as the leakage inductance $L_{lk}$ of the transformer and the firing angle $\alpha$ are assumed to be zero. Moreover, the DC bus inductance is assumed to have infinite value ($L_d = \infty$) making the output DC current constant. The three bridges are connected to the same wye primary winding while the other side of transformer is divided into two winding with Z connection and third winding with wye connection. As a result of this configuration, 20 degree phase shift angle between the three winding currents can be obtained. This type of configuration results in elimination of harmonic current of order $5^{th}$,$7^{th}$, $11^{th}$ and 13th which are the weightiest harmonics that can appear in the electric grid. Consequently, the resultant THD would be around 3.54% compared to 12 % for the 12-pulse Rectifier Bridge and 31% for the single 6-pulse bridge.

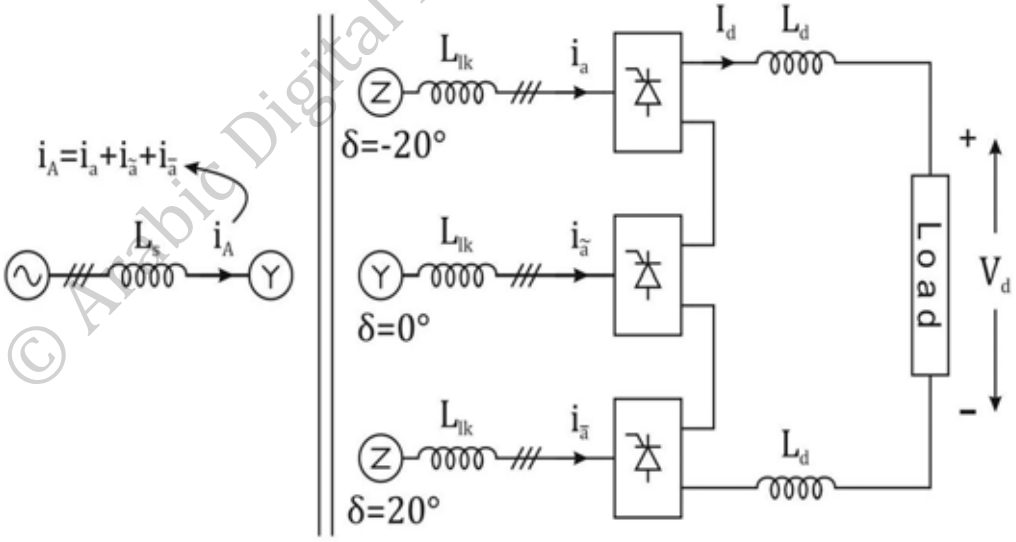


**Fig. 3.5** Simplified circuit diagram of a 24-pulse thyristor rectifier.

The THD of the line side current $i_A$ of the 18-pulse rectifier bridge is only 3.54 % while the THD of the line side current $i_A$ of the 12-pulse rectifier bridge is 15.3 %. On the other hand, the THD of the line side current of the 6-pulse rectifier bridge is 31 % . It is clearly noticeable that the reduction 24-pulse bridge offers, satisfies IEEE standards [3]. Form the previous discussion it can be concluded that the higher number of pulses the lower the line current distortion is. Additionally, when using higher pulses the need for AC side filters as well as DC-side filter will be diminished. The next chapter introduces the simulation results for the performance of the proposed method for line side current distortion estimation in terms of firing angle variation and taking into consideration the inductances of the source, line and transformer.

# CHAPTER FOUR:

## Simulation Results and Discussion

# Chapter Four: Results and Discussion

Three cases were conducted and simulated using MATLAB software. M. file code for 6-pulse rectifier bridge driving a separately excited DC motor is explained in Appendix. Assuming 3-phase balanced system, neither third nor even harmonics will show up during the simulation. Moreover, only the $I_5^{th}, I_7^{th}, I_{11}^{th}$ and $I_{13}^{th}$ will be taking into account when doing calculations since they represent the weightiest harmonics that could appear in a 6-pulse rectifier bridge [2].

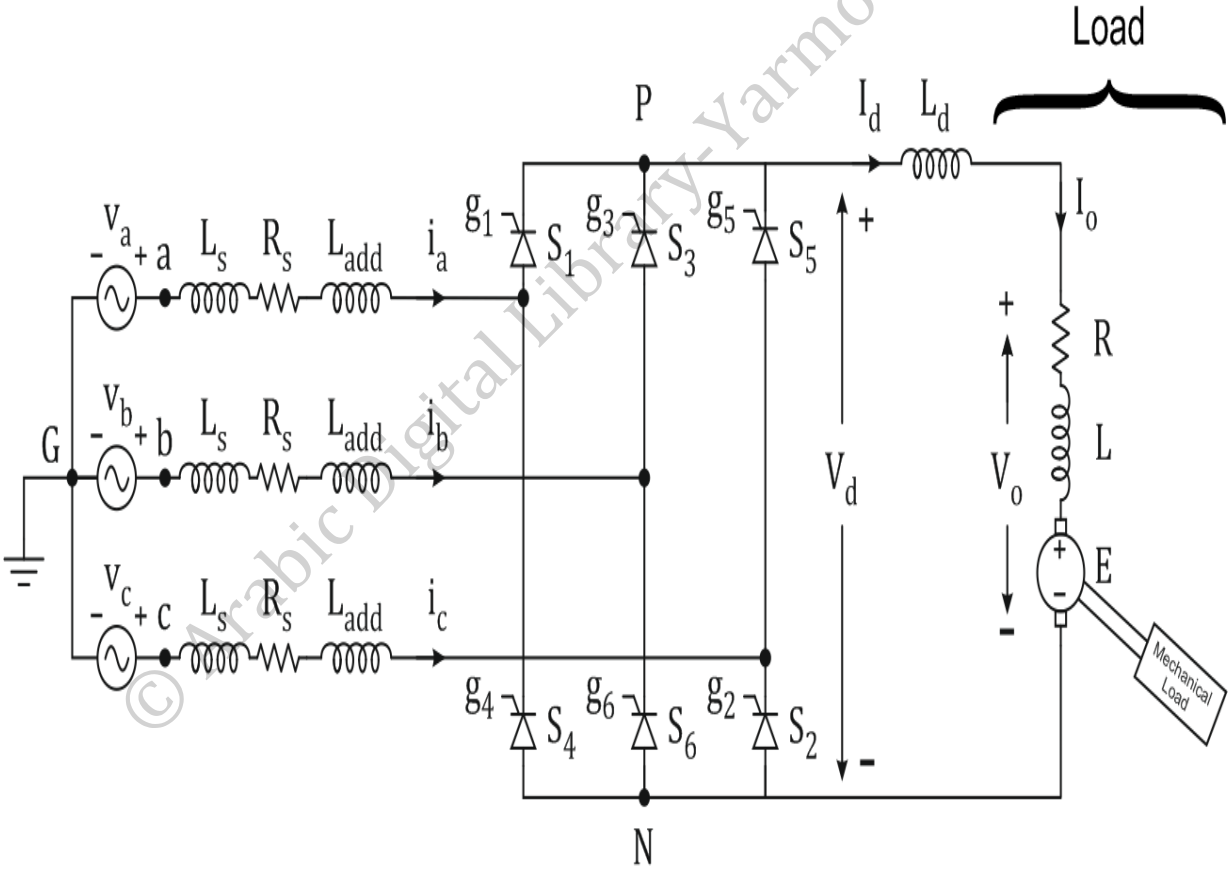


**Fig. 4.**1 Schematic of the modeled system.

Multiple simulations have been run independently varying one of the following parameters:

- Additional AC inductance $L_{add}$, from 0.2 to 1.2 $mH$.

- Additional DC-link inductance $L_d$ from 0.2 to 1.2 $mH$.
- Load, between 25% to 100% of the nominal load.

Then the results are stored in tables to calculate THDi.

## 4.1 Practical three-phase 6-pulse Bridge Rectifier

### 4.1.1 The effect of source inductance on circuit performance

Any AC source has an internal inductance and resistance plus the inductance and resistance of the cable that connects the source to the circuit. Therefore, we have to take the total inductance into consideration during analysis and modeling. Because the current passing through an inductance does not change instantly, it will require sometime to charge and discharge the inductor. This time depend on the time constant of the circuit. Consequently, the shapes of waveforms will get affected and as a result the average value of the output voltage will decrease because during commutation period $u$, the average output voltage is zero. Commutation definition is given in [28] which state that, commutation is the interval that we transfer load current from one switch to another with the presence of source inductance $L_s$.

To represent a practical three-phase source, the resistance and inductance values of the line should be specified. As a rule of thumb, the short circuit power $P_{sc}$ absorbed by the impedance source has to be 20 times higher than the drive nominal power [30]. Assuming stiff power system, as a result, the short circuit power is chosen to be 25 times higher than the nominal drive power:

$$P_{sc} = 25 \times \text{Nominal Drive Power} \tag{4.1}$$
$$= 25 \times 200\ hp \times 746 = 3.73\ [Mw]$$

The source impedance can be calculated as follows:

$$Z = \frac{V_{LL}^2}{P_{sc}} = \frac{460^2}{3.73 \times 10^6} = 0.0567\ [\Omega] \tag{4.2}$$

Usually, the $\frac{X}{R}$ ratio is 10 for industrial plants. $R$ and $L$ can be calculated as follows:

$$R = \frac{Z}{r} = \frac{0.0567}{10} = 0.00567\ [\Omega] \tag{4.3}$$

$$L = \frac{Z}{\omega} = \frac{0.0567}{2\pi f} = 0.18\ [mH] \tag{4.4}$$

**Table 4.1** Drive Specifications

| **200 HP Drive Specifications** | | |
|---|---|---|
| Drive Input Voltage | | |
| Amplitude 460 V (Line-to-Line) | frequency 50 Hz | |
| Motor Nominal Value | | |
| Power 200 HP | speed 1750 r.p.m | Voltage 500 V |

## 4.2 Simulation Results

From the simulation and at load equals to 100 % , $L_{add} = 0$ , the fundamental current is equal to $I_1 = 329.4\ A$.

### 4.2.1 Case study 1. Variation of firing angle vs. $L_{add}$

1. In this case, the parameters are as follows:

$L_s = 0.18\,mH, R = 0.00567\,\Omega$, with additional AC inductance $L_{add} = 0.2\,mH$, without DC inductance $L_d$ and the load torque $T_{Load}$=100%.

**Table 4.2** Harmonic Currents and $THD_i$% Values for Different Firing Angles and $L_{add} = 0.2\,mH$.

| Firing Angle | $I_1\,[A]$ | $I_5\,[A]$ | $I_7\,[A]$ | $I_{11}\,[A]$ | $I_{13}\,[A]$ | $THD_i$ % | $THD_v$% |
|---|---|---|---|---|---|---|---|
| $0^\circ$ | 315 | 52.9 | 17.2 | 7.4 | 3.5 | 18.8 | 13.5 |
| 30 | 278.15 | 62.6 | 19.25 | 12.6 | 9.7 | 25.3 | 17.3 |
| $45^\circ$ | 232.75 | 62.7 | 15 | 13.16 | 9.6 | 30 | 16.4 |
| $60^\circ$ | 160 | 57.55 | 13.35 | 15.27 | 3.4 | 38.7 | 15.5 |
| $75^\circ$ | 81.5 | 40.9 | 24.4 | 5.3 | 8.4 | 57 | 13.2 |

Fig 4.2 shows the simulation results of the harmonic currents when varying the firing angle and $L_{add} = 0.2\,mH$.

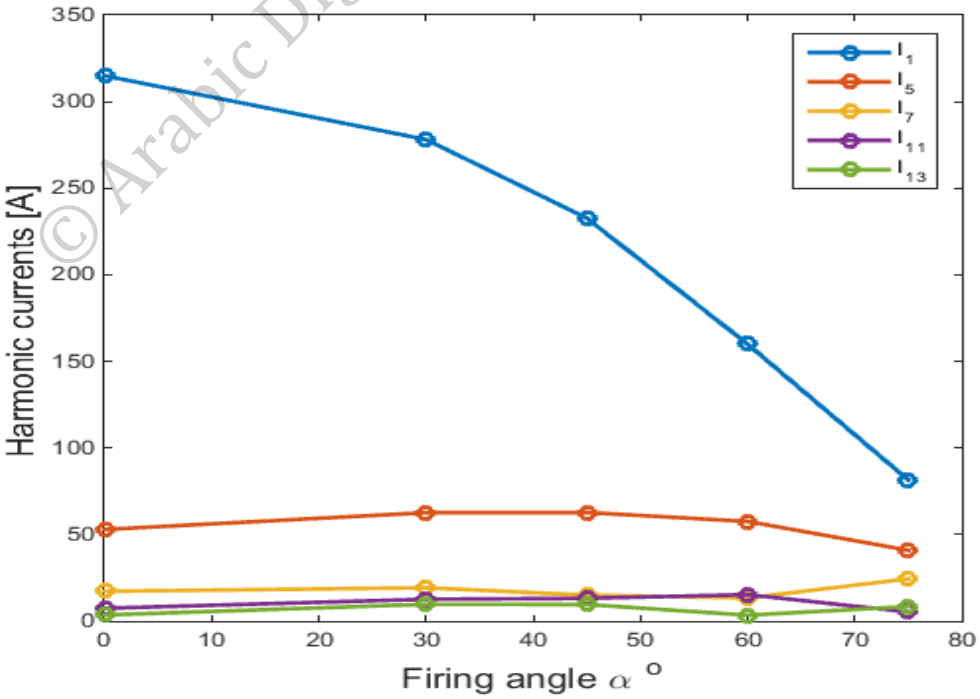


**Fig. 4.2** Simulated harmonic currents in terms of firing angle variation and $L_{add} = 0.2\,mH$

2. In this case, the parameters are as follows:

$L_s = 0.18\ mH, R = 0.00567\ \Omega$, with additional AC inductance $L_{add} = 0.4\ mH$, without DC inductance $L_d$ and the load torque $T_{Load}$=100%.

**Table 4.3** Harmonic Currents and $THD_i\%$ Values for Different Firing Angles and $L_{add} = 0.4\ mH$.

| Firing Angle | $I_1\ [A]$ | $I_5\ [A]$ | $I_7\ [A]$ | $I_{11}\ [A]$ | $I_{13}\ [A]$ | $THD_i\%$ | $THD_v\%$ |
|---|---|---|---|---|---|---|---|
| $0^\circ$ | 299 | 38.35 | 14.4 | 6.16 | 3.5 | 14.7 | 15.5 |
| 30 | 248.15 | 46 | 21.15 | 3.97 | 5.5 | 20.4 | 19.6 |
| $45^\circ$ | 209.5 | 50.75 | 14.25 | 11.6 | 8 | 26.15 | 21.7 |
| $60^\circ$ | 150 | 45.75 | 5.54 | 12 | 3.75 | 32.25 | 18.6 |
| $75^\circ$ | 71.5 | 35 | 13.5 | 4.8 | 4.25 | 49.4 | 14.5 |

Fig 4.3 shows the simulation results of the harmonic currents when varying the firing angle and $L_{add} = 0.4\ mH$

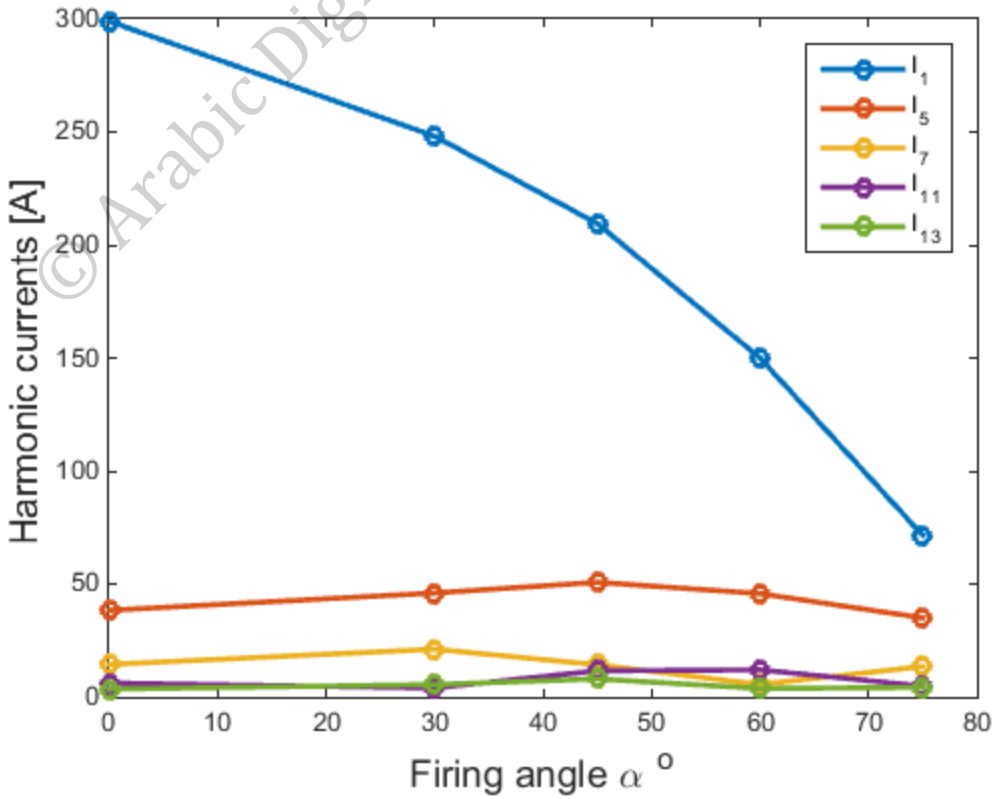


**Fig. 4.3** Simulated harmonic currents in terms of firing angle variation and $L_{add} = 0.4\ mH$

3. In this case, the parameters are as follows:

$L_s = 0.18\ mH, R = 0.00567\ \Omega$, with additional AC inductance $L_{add} = 0.6\ mH$, without DC inductance $L_d$ and the load torque $T_{Load}$=100%.

**Table 4.4** Harmonic Currents and $THD_i\%$ Values for Different Firing Angles and $L_{add} = 0.6\ mH$.

| Firing Angle | $I_1\ [A]$ | $I_5\ [A]$ | $I_7\ [A]$ | $I_{11}\ [A]$ | $I_{13}\ [A]$ | $THD_i\%$ | $THD_v\%$ |
|---|---|---|---|---|---|---|---|
| $0^\circ$ | 278.7 | 28.9 | 10.95 | 5.25 | 3.34 | 11.8 | 16.3 |
| 30 | 240.45 | 38.8 | 18.35 | 2.45 | 2.75 | 18.15 | 21.7 |
| $45^\circ$ | 191 | 43.8 | 12.2 | 8.8 | 5.85 | 24.6 | 24.4 |
| $60^\circ$ | 142.15 | 39.9 | 5.9 | 9.95 | 4.45 | 29.7 | 22 |
| $75^\circ$ | 66.35 | 32.5 | 9.6 | 4.48 | 2.85 | 45.7 | 17.2 |

Fig 4.4 shows the simulation results of the harmonic currents when varying the firing angle and $L_{add} = 0.6\ mH$

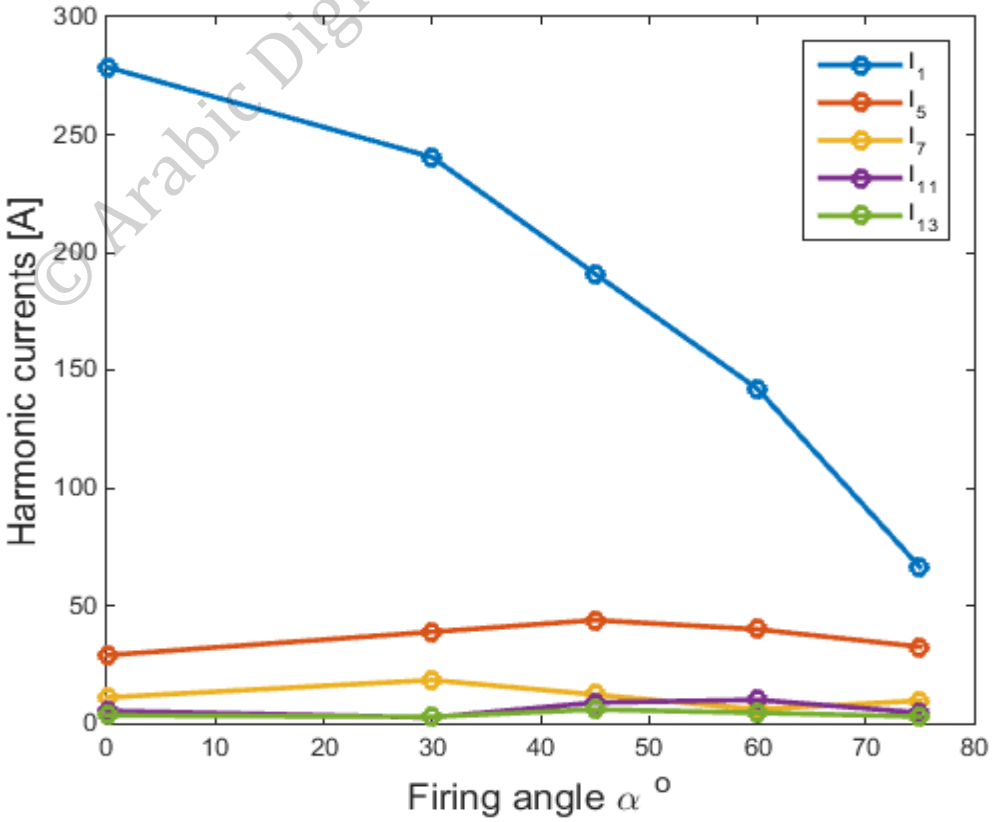


**Fig. 4.4** Simulated harmonic currents in terms of firing angle variation and $L_{add} = 0.6\ mH$

4. In this case, the parameters are as follows:

$L_s = 0.18\ mH, R = 0.00567\ \Omega$, with additional AC inductance $L_{add} = 0.8\ mH$, without DC inductance $L_d$ and the load torque $T_{Load}$=100%.

**Table 4.5** Harmonic Currents and $THD_i\%$ Values for Different Firing Angles and $L_{add} = 0.8\ mH$.

| Firing Angle | $I_1\ [A]$ | $I_5\ [A]$ | $I_7\ [A]$ | $I_{11}\ [A]$ | $I_{13}\ [A]$ | $THD_i\%$ | $THD_v\%$ |
|---|---|---|---|---|---|---|---|
| $0^\circ$ | 250.25 | 22.35 | 8.45 | 4.1 | 2.65 | 9.5 | 16.9 |
| 30 | 222.5 | 33.95 | 15.5 | 2.7 | 1.23 | 16.9 | 23.6 |
| $45^\circ$ | 179.75 | 38 | 11.95 | 6.7 | 4.65 | 22.88 | 26.5 |
| $60^\circ$ | 134.75 | 37.5 | 6.9 | 8.15 | 4.65 | 27.7 | 25.6 |
| $75^\circ$ | 62 | 30.5 | 7 | 4.42 | 1.9 | 42.9 | 19.6 |

Fig 4.5 shows the simulation results of the harmonic currents when varying the firing angle and $L_{add} = 0.8\ mH$

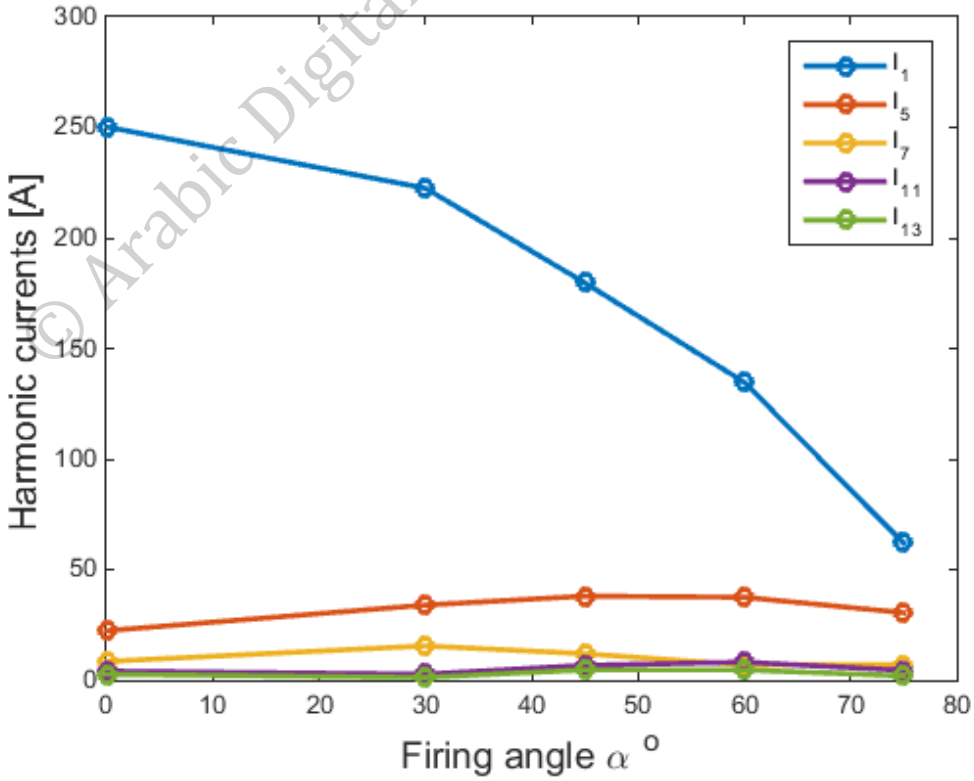


**Fig. 4.5** Simulated harmonic currents in terms of firing angle variation and $L_{add} = 0.8\ mH$

5. In this case, the parameters are as follows:

$L_s = 0.18\ mH, R = 0.00567\ \Omega$, with additional AC inductance $L_{add} = 1\ mH$, without DC inductance $L_d$ and the load torque $T_{Load}$=100%.

**Table 4.6** Harmonic Currents and $THD_i\%$ Values for Different Firing Angles and $L_{add} = 1\ mH$.

| Firing Angle | $I_1\ [A]$ | $I_5\ [A]$ | $I_7\ [A]$ | $I_{11}\ [A]$ | $I_{13}\ [A]$ | $THD_i\%$ | $THD_v\%$ |
|---|---|---|---|---|---|---|---|
| $0^\circ$ | 236.25 | 17.9 | 6.65 | 3.25 | 2 | 7.9 | 17.2 |
| 30 | 207 | 29.8 | 13 | 2.95 | 0.6 | 16 | 24.7 |
| $45^\circ$ | 171.5 | 33.2 | 12 | 3.6 | 4.65 | 21 | 27.7 |
| $60^\circ$ | 132.5 | 31.44 | 7.6 | 6.6 | 4.5 | 26.1 | 26 |
| $75^\circ$ | 58.5 | 25.9 | 5.15 | 4.35 | 1.3 | 40.8 | 19.8 |

Fig 4.6 shows the simulation results of the harmonic currents when varying the firing angle and $L_{add} = 1\ mH$

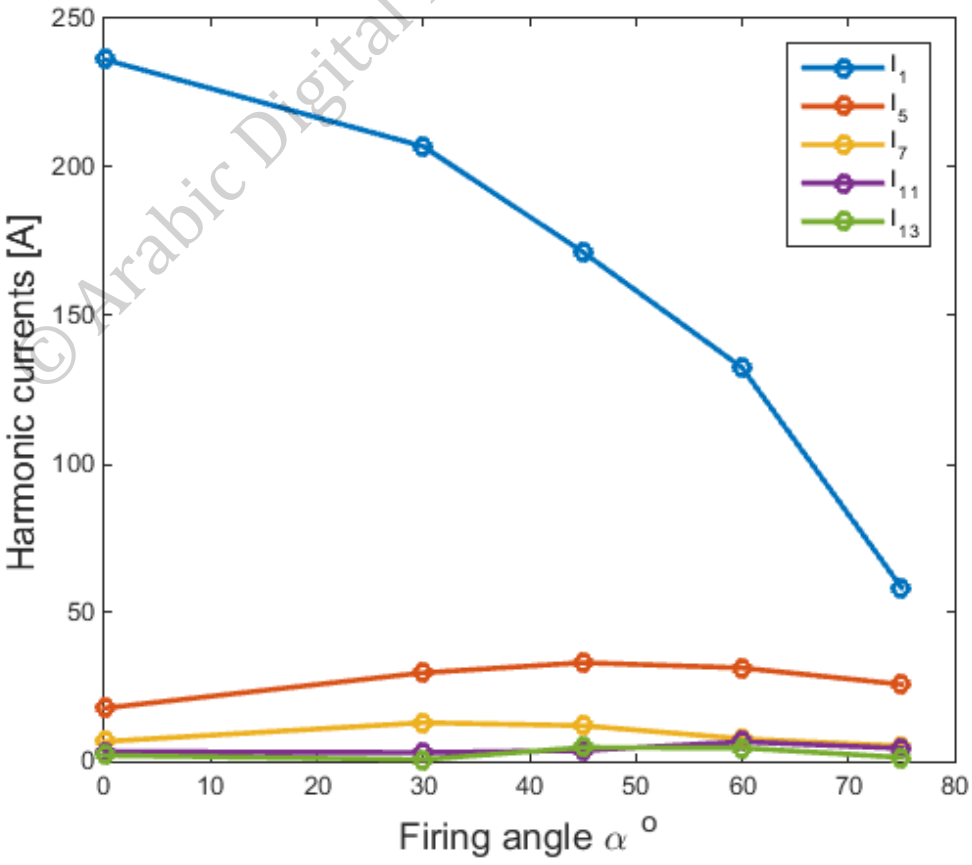


**Fig. 4.6** Simulated harmonic currents in terms of firing angle variation and $L_{add} = 1\ mH$

6. In this case, the parameters are as follows:

$L_s = 0.18\ mH, R = 0.00567\ \Omega$, with additional AC inductance $L_{add} = 1.2\ mH$, without DC inductance $L_d$ and the load torque $T_{Load}$=100%.

**Table 4.7** Harmonic Currents and $THD_i\%$ Values for Different Firing Angles and $L_{add} = 1.2\ mH$.

| Firing Angle | $I_1\ [A]$ | $I_5\ [A]$ | $I_7\ [A]$ | $I_{11}\ [A]$ | $I_{13}\ [A]$ | $THD_i\%$ | $THD_v\%$ |
|---|---|---|---|---|---|---|---|
| $0^\circ$ | 205.55 | 14.8 | 5.4 | 2.7 | 1.65 | 6.8 | 18.3 |
| 30 | 173.95 | 26.35 | 11 | 3.28 | 0.55 | 15.4 | 25 |
| $45^\circ$ | 154.5 | 29 | 11.8 | 1.85 | 2.45 | 19.3 | 28 |
| $60^\circ$ | 122 | 28.25 | 7.95 | 5.2 | 4.15 | 24.7 | 27.6 |
| $75^\circ$ | 56 | 27.25 | 3.85 | 4.2 | 0.88 | 39 | 24 |

Fig 4.7 shows the simulation results of the harmonic currents when varying the firing angle and $L_{add} = 1.2\ mH$

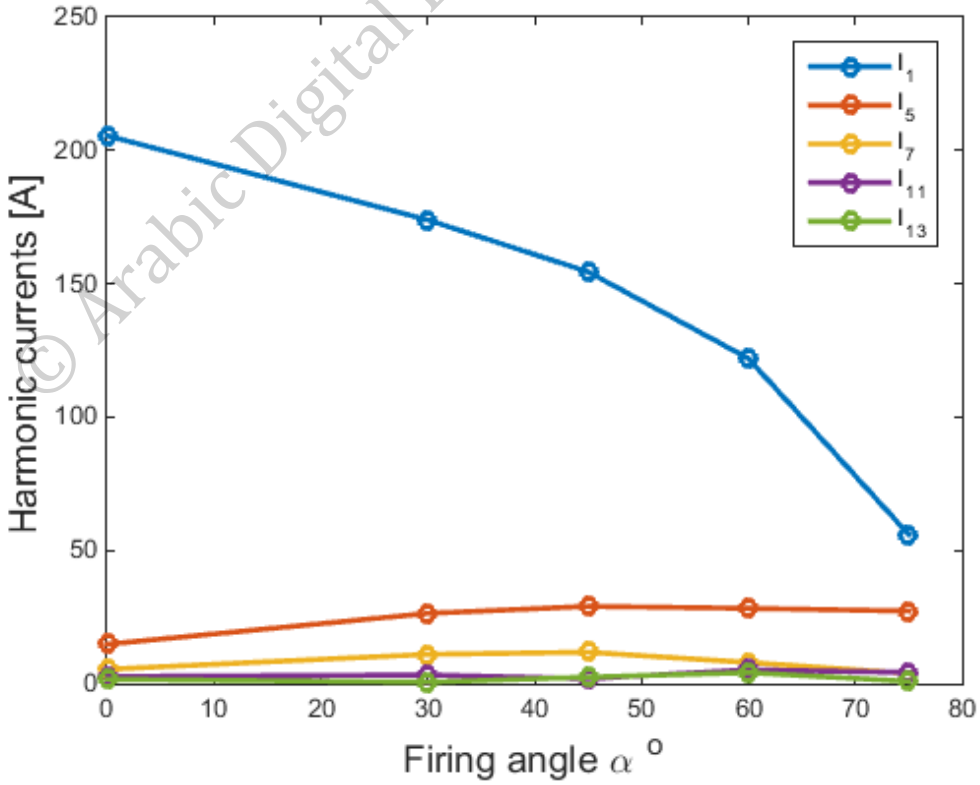


**Fig. 4.7** Simulated harmonic currents in terms of firing angle variation and $L_{add} = 1.2\ mH$

The fundamental current frequency is equal to $f_1 = 50\ Hz$ and the magnitude of the impedance of inductance $L$ at the fundamental frequency is equal to:

$$Z_1 = \omega_1 L = 2\pi f_1 L \tag{4.5}$$

Since, harmonics are multiples of the fundamental frequency that means higher harmonic current order has higher frequency, for instance, the fifth harmonic current frequency passes through the inductor is equal to:

$$f_5 = 5 \times f_1$$

And the corresponding impedance is equal to:

$$Z_5 = w_5 L = 2\pi f_5 L = 2\pi(5f_1)L = 5Z_1$$

As shown in equation (4.8) the higher the harmonic order the larger the impedance is. In other words, higher harmonic orders will result in larger impedances that will suppress harmonic currents from passing through them. In the same way, increasing the AC inductance will have a slight effect on the impedance at the fundamental frequency nevertheless; the effect will be huge on the impedances of higher harmonic orders.

Fig 4.8 shows the simulation results of the THDi for different inductance values $L_{add}$ at various firing angle $\alpha$.

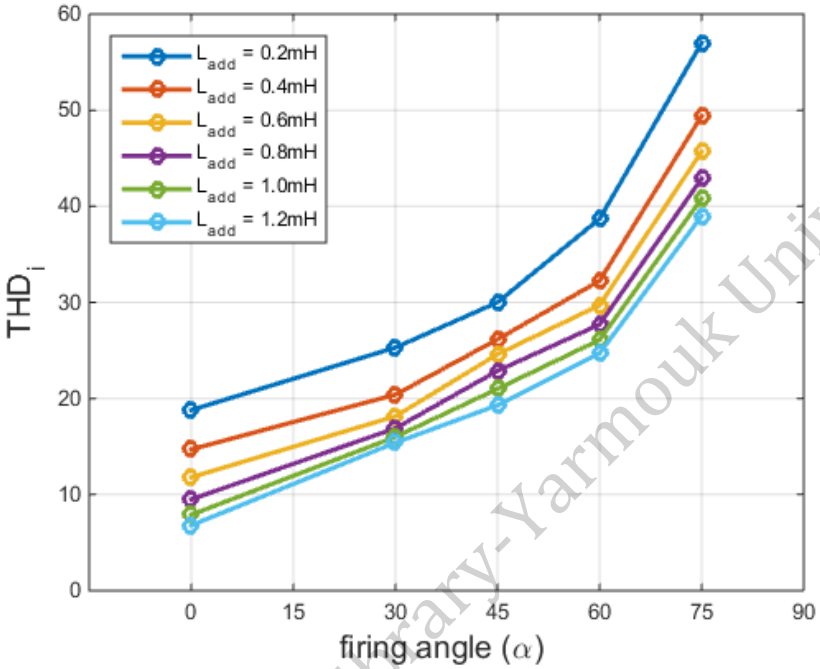


**Fig. 4.8** Firing angle vs. $L_{add}$ Variation.

### 4.2.2 Case study 2. Variation of firing angle vs. $L_d$

1. In this case, the parameters are as follows:

$L_s = 0.18\ mH, R = 0.00567\ \Omega$, without additional AC inductance, with DC inductance $L_d = 0.2\ mH$ and the load torque $T_{Load}$=100%.

**Table 4.8** Harmonic Currents and $THD_i\%$ Values for Different Firing Angles and $L_d = 0.2\ mH$.

| Firing Angle | $I_1\ [A]$ | $I_5\ [A]$ | $I_7\ [A]$ | $I_{11}\ [A]$ | $I_{13}\ [A]$ | $THD_i\%$ | $THD_v\%$ |
|---|---|---|---|---|---|---|---|
| $0^\circ$ | 316.6 | 77.2 | 27.3 | 17.4 | 7.5 | 26.5 | 9.5 |
| 30 | 298.95 | 67 | 42.57 | 27.1 | 19 | 31.8 | 10.5 |
| $45^\circ$ | 248.35 | 65.3 | 17 | 11.16 | 13.6 | 36.2 | 7.7 |
| $60^\circ$ | 168 | 59 | 16.5 | 12.27 | 9.4 | 44.2 | 7 |
| $75^\circ$ | 86.5 | 43 | 33.2 | 8.3 | 9.4 | 64 | 6.9 |

Fig 4.9 shows the simulation results of the harmonic currents when varying the firing angle and $L_d = 0.2\ mH$.

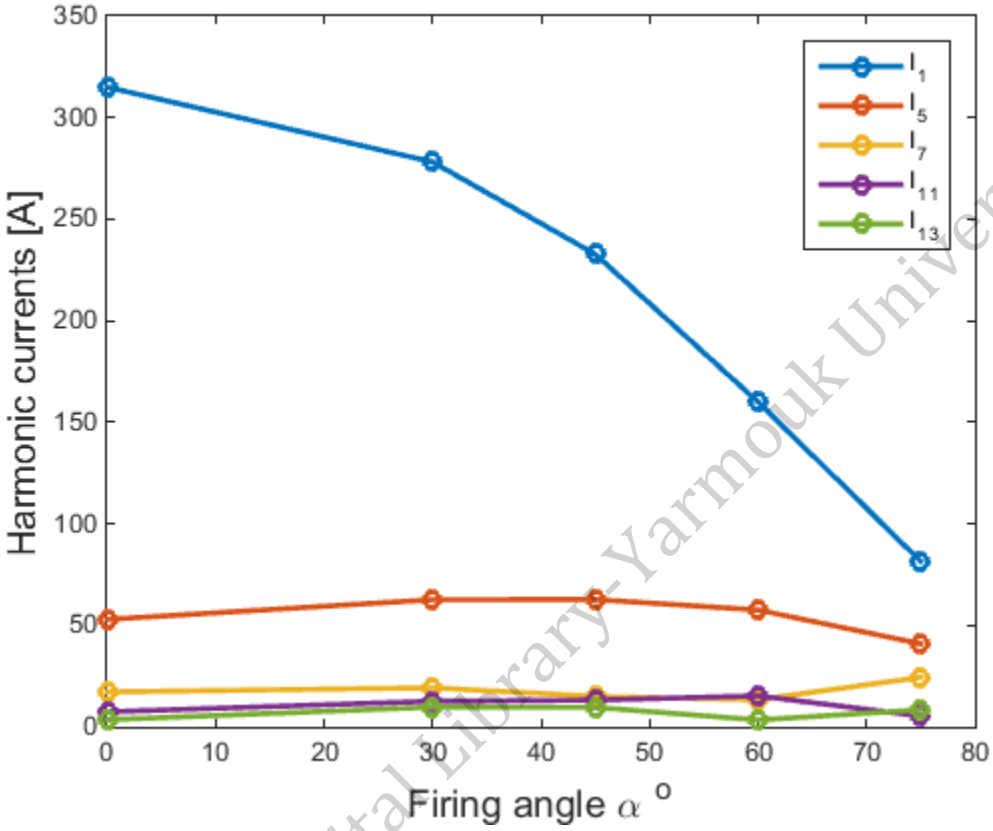


**Fig. 4.9** Simulated harmonic currents in terms of firing angle variation and $L_d = 0.2\ mH$

2. In this case, the parameters are as follows:

$L_s = 0.18\ mH, R = 0.00567\ \Omega$, without additional AC inductance, with DC inductance $L_d = 0.4\ mH$ and the load torque $T_{Load}$=100%.

**Table 4.9** Harmonic Currents and $THD_i\%$ Values for Different Firing Angles and $L_d = 0.4\ mH$.

| Firing Angle | $I_1\ [A]$ | $I_5\ [A]$ | $I_7\ [A]$ | $I_{11}\ [A]$ | $I_{13}\ [A]$ | $THD_i\%$ | $THD_v\%$ |
|---|---|---|---|---|---|---|---|
| $0^\circ$ | 310.6 | 63.3 | 14.4 | 12.16 | 6.5 | 20.5 | 7.8 |
| 30 | 265.8 | 61 | 21.15 | 8.97 | 5.5 | 27.8 | 7.6 |
| $45^\circ$ | 225.1 | 55.75 | 19.25 | 11.6 | 8 | 30.2 | 7.4 |
| $60^\circ$ | 158 | 45.75 | 8.54 | 12 | 6.75 | 38.2 | 6 |
| $75^\circ$ | 76.4 | 35 | 13.5 | 7.8 | 6.25 | 55 | 4.8 |

Fig 4.10 shows the simulation results of the harmonic currents when varying the firing angle and $L_d = 0.4\,mH$.

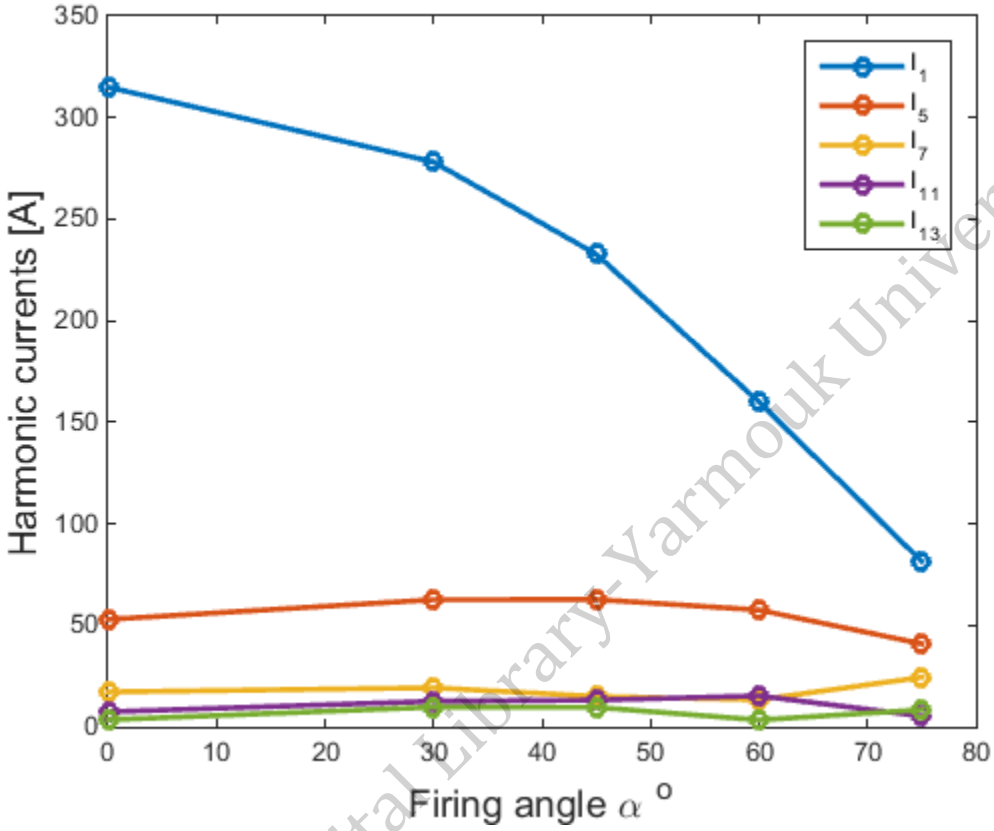


**Fig. 4.10** Simulated harmonic currents in terms of firing angle variation and $L_d = 0.4\,mH$

3. In this case, the parameters are as follows:

$L_s = 0.18\,mH, R = 0.00567\,\Omega$, without additional AC inductance, with DC inductance $L_d = 0.6\,mH$ and the load torque $T_{Load}$=100%.

**Table 4.10** Harmonic Currents and $THD_i\%$ Values for Different Firing Angles and $L_d = 0.6\,mH$.

| Firing Angle | $I_1\,[A]$ | $I_5\,[A]$ | $I_7\,[A]$ | $I_{11}\,[A]$ | $I_{13}\,[A]$ | $THD_i\%$ | $THD_v\%$ |
|---|---|---|---|---|---|---|---|
| $0^\circ$ | 300.2 | 58 | 10.95 | 5.25 | 3.34 | 17.4 | 6.3 |
| 30 | 261.1 | 52 | 18.35 | 2.45 | 2.75 | 25.8 | 6.2 |
| $45^\circ$ | 206.6 | 56 | 12.2 | 8.8 | 5.85 | 28.2 | 6.6 |
| $60^\circ$ | 150.15 | 39.9 | 5.9 | 9.95 | 4.45 | 35.7 | 5 |
| $75^\circ$ | 71.25 | 33 | 9.6 | 4.48 | 2.85 | 50.8 | 3.9 |

Fig 4.11 shows the simulation results of the harmonic currents when varying the firing angle and $L_d = 0.6\,mH$.

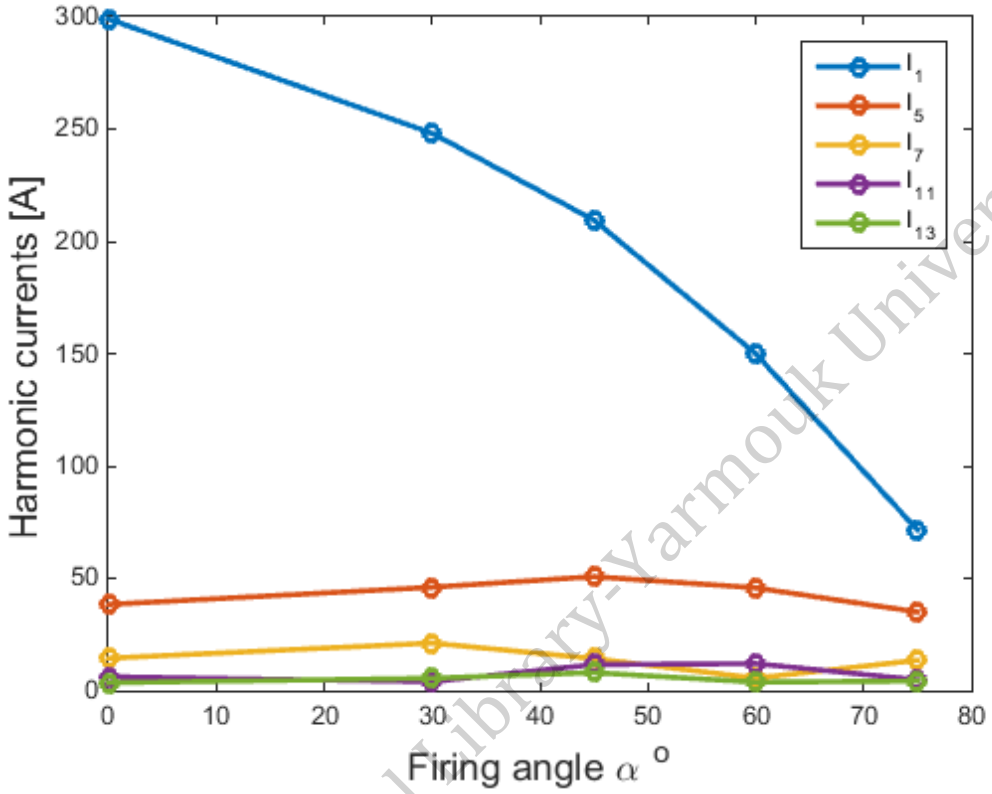


**Fig. 4.11** Simulated harmonic currents in terms of firing angle variation and $L_d = 0.6\,mH$

4. In this case, the parameters are as follows:

$L_s = 0.18\,mH, R = 0.00567\,\Omega$, without additional AC inductance, with DC inductance $L_d = 0.8\,mH$ and the load torque $T_{Load}$=100%.

**Table 4.11** Harmonic Currents and $THD_i\%$ Values for Different Firing Angles and $L_d = 0.8\,mH$.

| Firing Angle | $I_1\,[A]$ | $I_5\,[A]$ | $I_7\,[A]$ | $I_{11}\,[A]$ | $I_{13}\,[A]$ | $THD_i\%$ | $THD_v\%$ |
|---|---|---|---|---|---|---|---|
| $0^\circ$ | 271.75 | 45.16 | 8.45 | 4.1 | 2.65 | 15.1 | 5 |
| 30 | 243.15 | 39.95 | 15.5 | 2.7 | 1.23 | 24.55 | 4.8 |
| $45^\circ$ | 195.35 | 38 | 11.95 | 6.7 | 4.65 | 26.48 | 4.85 |
| $60^\circ$ | 142.7 | 37.5 | 6.9 | 8.15 | 4.65 | 33.7 | 4.7 |
| $75^\circ$ | 66.9 | 31.2 | 7 | 4.42 | 1.9 | 48 | 3.6 |

Fig 4.12 shows the simulation results of the harmonic currents when varying the firing angle and $L_d = 0.8\,mH$.

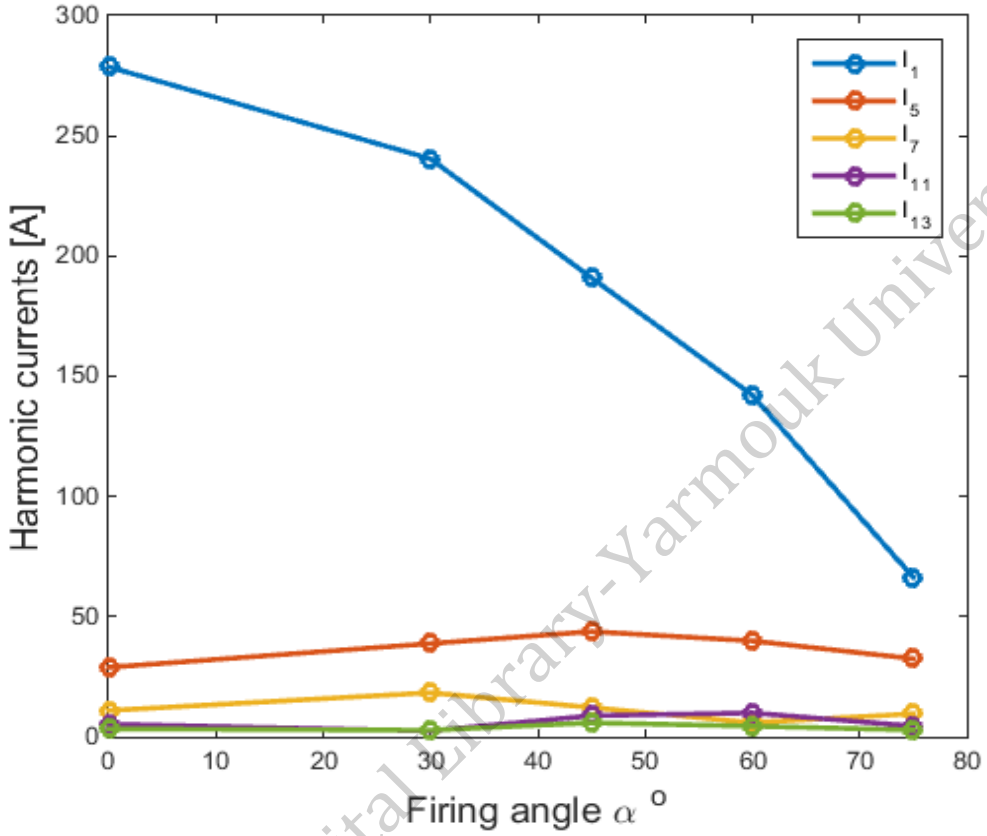


**Fig. 4.12** Simulated harmonic currents in terms of firing angle variation and $L_d = 0.8\,mH$

5. In this case, the parameters are as follows:

$L_s = 0.18\,mH, R = 0.00567\,\Omega$, without additional AC inductance, with DC inductance $L_d = 1\,mH$ and the load torque $T_{Load}$=100%.

**Table 4.12** Harmonic Currents and $THD_i\%$ Values for Different Firing Angles and $L_d = 1\,mH$.

| Firing Angle | $I_1\,[A]$ | $I_5\,[A]$ | $I_7\,[A]$ | $I_{11}\,[A]$ | $I_{13}\,[A]$ | $THD_i\%$ | $THD_v\%$ |
|---|---|---|---|---|---|---|---|
| $0^\circ$ | 252.75 | 42.8 | 6.65 | 3.25 | 2 | 13.5 | 4.7 |
| 30 | 227.65 | 37.7 | 13 | 2.95 | 0.6 | 23.65 | 4.5 |
| $45^\circ$ | 187.1 | 34.2 | 12 | 3.6 | 4.65 | 24.75 | 4.3 |
| $60^\circ$ | 140 | 31.44 | 7.6 | 6.6 | 4.5 | 32.1 | 4 |
| $75^\circ$ | 63.8 | 30.9 | 5.15 | 4.35 | 1.3 | 45.9 | 3.5 |

Fig 4.13 shows the simulation results of the harmonic currents when varying the firing angle and $L_d = 1\ mH$.

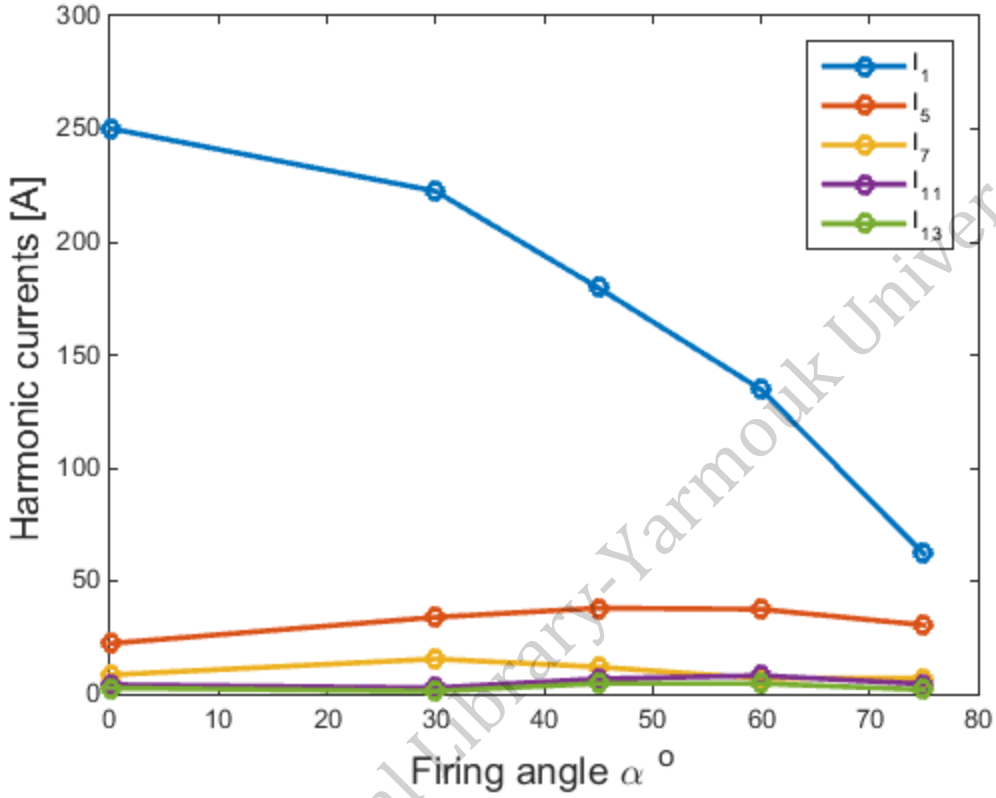


**Fig. 4.13** Simulated harmonic currents in terms of firing angle variation and $L_d = 1\ mH$

6. In this case, the parameters are as follows:

$L_s = 0.18\ mH, R = 0.00567\ \Omega$, without additional AC inductance, with DC inductance $L_d = 1.2\ mH$ and the load torque $T_{Load}$=100%.

**Table 4.13** Harmonic Currents and $THD_i\%$ Values for Different Firing Angles and $L_d = 1.2\ mH$.

| Firing Angle | $I_1\ [A]$ | $I_5\ [A]$ | $I_7\ [A]$ | $I_{11}\ [A]$ | $I_{13}\ [A]$ | $THD_i\%$ | $THD_v\%$ |
|---|---|---|---|---|---|---|---|
| $0^\circ$ | 207 | 30.8 | 5.4 | 2.7 | 1.65 | 12.4 | 3.4 |
| 30 | 179.5 | 33.35 | 11 | 3.28 | 0.55 | 21.65 | 3.9 |
| $45^\circ$ | 138.1 | 29 | 11.8 | 1.85 | 2.45 | 23 | 3.6 |
| $60^\circ$ | 109.5 | 28.25 | 7.95 | 5.2 | 4.15 | 30.7 | 3.6 |
| $75^\circ$ | 61.5 | 24.25 | 3.85 | 4.2 | 0.88 | 44.1 | 2.8 |

Fig 4.14 shows the simulation results of the harmonic currents when varying the firing angle and $L_d = 1.2\ mH$.

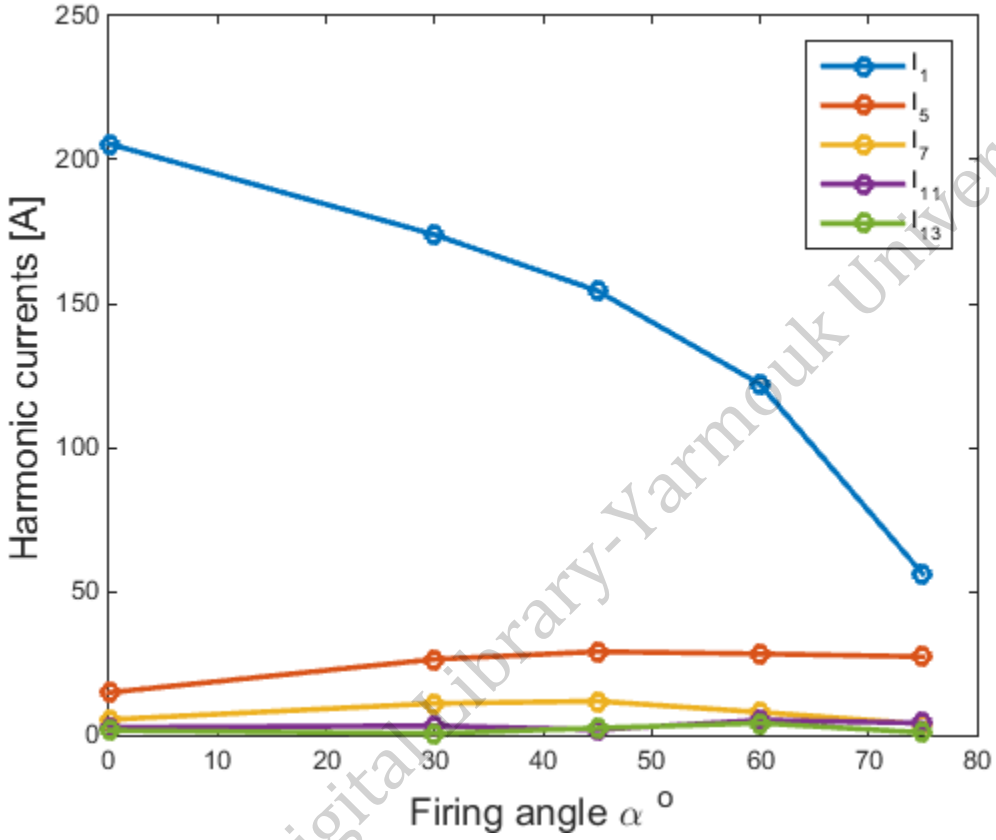


**Fig. 4.14** Simulated harmonic currents in terms of firing angle variation and $L_d = 1.2\ mH$



Since the current in the inductor does not change instantaneously, higher DC-link inductor filter decreases the amount of ripple in the output current to make it more like DC, leading to reduction of harmonic currents at the input of the three phase rectifier bridge.

Fig.4.15 shows the simulation results of the THDi for different inductance values $L_d$ at various firing angle $\alpha$.

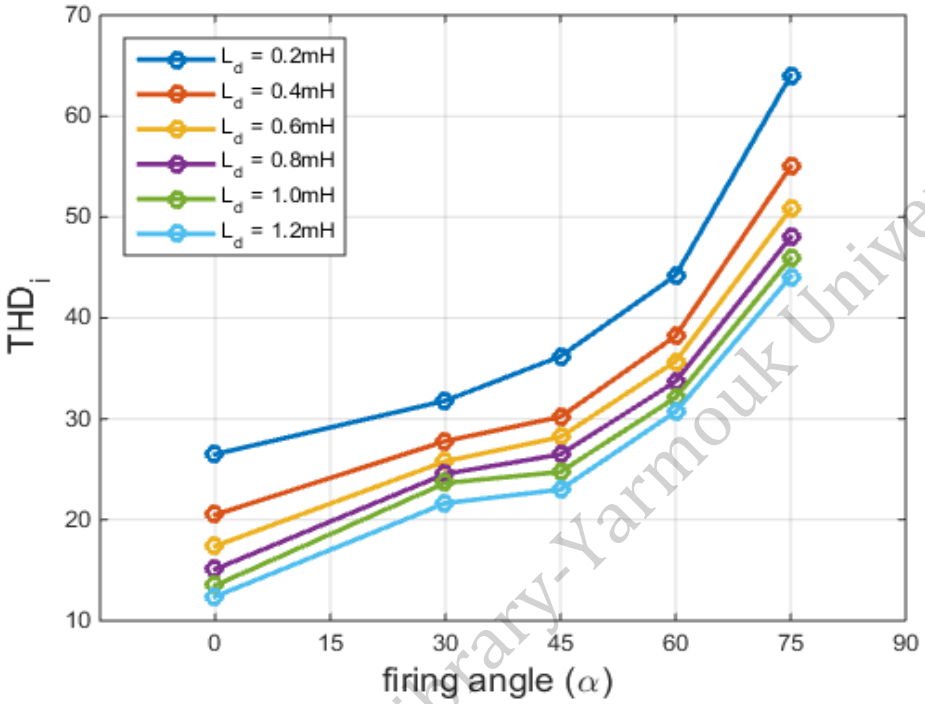


**Fig. 4.15** Firing angle Vs. $L_d$ Variation



### 4.2.3 Case study 3. Variation of firing angle vs. load

1. In this case, the parameters are as follows:

$L_s = 0.18\,mH, R = 0.00567\ \Omega$, without additional AC inductance or DC inductance $L_d$ and the load torque $T_{Load}$= 25%.

**Table 4.14** Harmonic Currents and $THD_i$% Values for Different Firing Angles and $T_{load} = 25\%$

| Firing Angle | $I_1\ [A]$ | $I_5\ [A]$ | $I_7\ [A]$ | $I_{11}\ [A]$ | $I_{13}\ [A]$ | $THD_i\%$ | $THD_v\%$ |
|---|---|---|---|---|---|---|---|
| $0^\circ$ | 96.67 | 24.15 | 9.14 | 9.1 | 4 | 30.2 | 3.7 |
| 30 | 53.55 | 21.6 | 8 | 7.4 | 2.4 | 85.8 | 3.1 |
| $45^\circ$ | 65.9 | 24.6 | 5.5 | 6.2 | 2.6 | 86.4 | 3.1 |
| $60^\circ$ | 71 | 28.7 | 7.3 | 7.3 | 3.1 | 90.9 | 3.7 |
| $75^\circ$ | 29.5 | 18.7 | 10.8 | 1.4 | 3.15 | 116.4 | 2.7 |

Fig 4.16 shows the simulation results of the harmonic currents when varying the firing angle and $T_{load} = 25\%$.

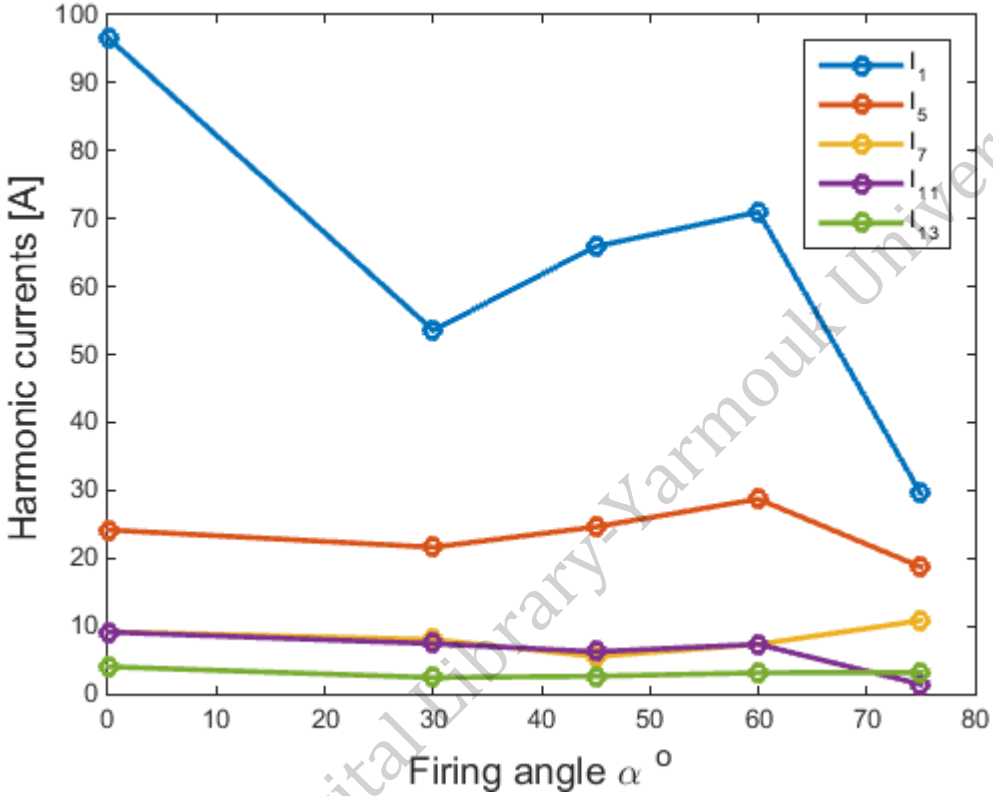


**Fig. 4.16** Simulated harmonic currents in terms of firing angle variation and $T_{load} = 25\%$.



2. In this case, the parameters are as follows:

$L_s = 0.18\,mH, R = 0.00567\ \Omega$, without additional AC inductance or DC inductance $L_d$ and the load torque $T_{Load}$= 50%.

**Table 4.15** Harmonic Currents and $THD_i\%$ Values for Different Firing Angles and $T_{load} = 50\%$

| Firing Angle | $I_1\ [A]$ | $I_5\ [A]$ | $I_7\ [A]$ | $I_{11}\ [A]$ | $I_{13}\ [A]$ | $THD_i\%$ | $THD_v\%$ |
|---|---|---|---|---|---|---|---|
| $0^\circ$ | 180.9 | 43.37 | 16.4 | 16.3 | 6.28 | 28.9 | 8 |
| 30 | 108.8 | 30.35 | 14.7 | 12.45 | 6 | 67.2 | 7.15 |
| $45^\circ$ | 96 | 34.9 | 10.7 | 10.88 | 6.34 | 87.3 | 6.2 |
| $60^\circ$ | 92.26 | 37.9 | 11.45 | 11.7 | 6.4 | 92.14 | 6.4 |
| $75^\circ$ | 40.65 | 26 | 14.9 | 4.1 | 5.9 | 116.8 | 5 |

Fig 4.17 shows the simulation results of the harmonic currents when varying the firing angle and $T_{load} = 50\%$.

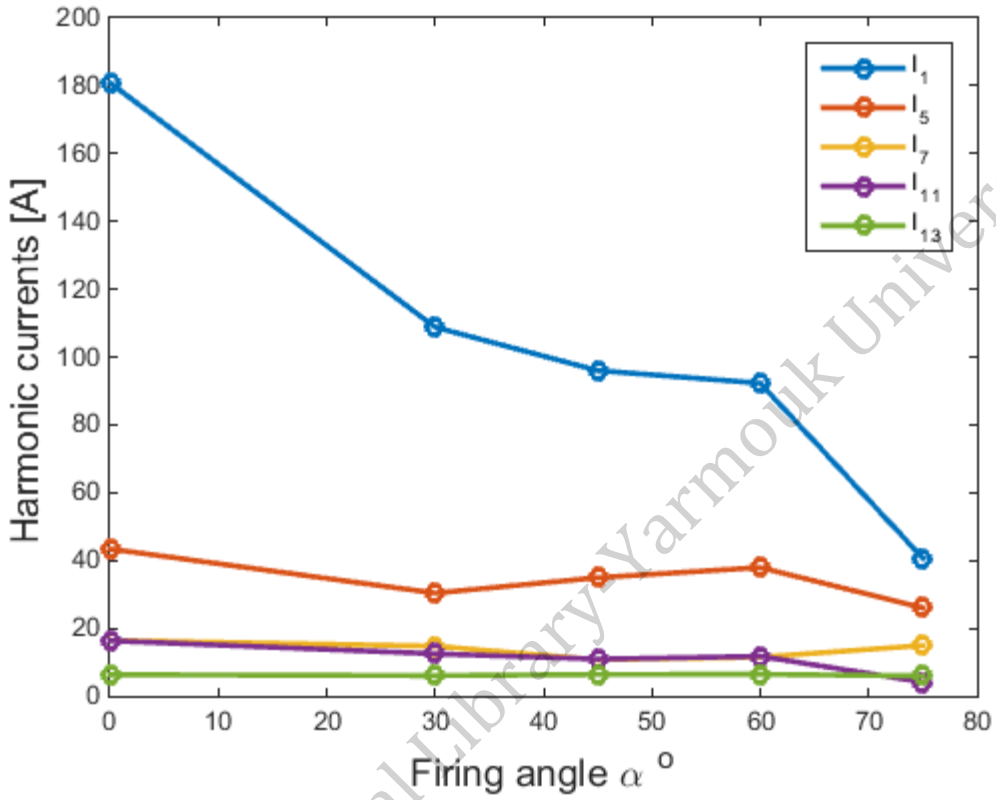


**Fig. 4.17** Simulated harmonic currents in terms of firing angle variation and $T_{load} = 50\%$.



3. In this case, the parameters are as follows:

$L_s = 0.18\,mH, R = 0.00567\ \Omega$, without additional AC inductance or DC inductance $L_d$ and the load torque $T_{Load}$= 75%.

**Table 4.16** Harmonic Currents and $THD_i\%$ Values for Different Firing Angles and $T_{load} = 75\%$

| Firing Angle | $I_1\ [A]$ | $I_5\ [A]$ | $I_7\ [A]$ | $I_{11}\ [A]$ | $I_{13}\ [A]$ | $THD_i\%$ | $THD_v\%$ |
|---|---|---|---|---|---|---|---|
| $0^\circ$ | 264 | 62 | 22.8 | 22.7 | 7.5 | 28 | 9.3 |
| 30 | 177.4 | 39.75 | 25 | 18.9 | 10.1 | 55.6 | 7.6 |
| $45^\circ$ | 123 | 42.9 | 16.9 | 15.14 | 9.4 | 85.9 | 6.6 |
| $60^\circ$ | 107.6 | 45.5 | 15.7 | 15.5 | 9.2 | 93.56 | 6.9 |
| $75^\circ$ | 53 | 34.9 | 20.5 | 7.2 | 8.9 | 119 | 7.6 |

Fig 4.18 shows the simulation results of the harmonic currents when varying the firing angle and $T_{load} = 75\%$.

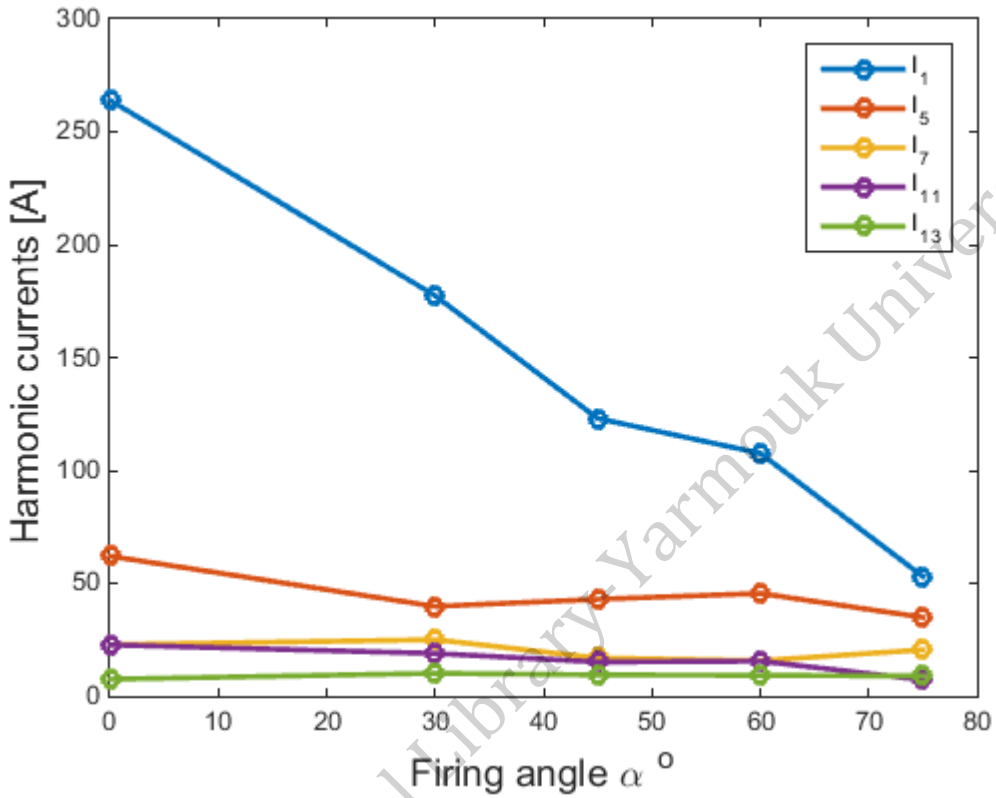


**Fig. 4.18** Simulated harmonic currents in terms of firing angle variation and $T_{load} = 75\%$.



4. In this case, the parameters are as follows:

$L_s = 0.18\ mH, R = 0.00567\ \Omega$, without additional AC inductance or DC inductance $L_d$ and the load torque $T_{Load}$= 100%.

**Table 4.17** Harmonic Currents and $THD_i\%$ Values for Different Firing Angles and $T_{load} = 100\%$

| Firing Angle | $I_1$ [A] | $I_5$ [A] | $I_7$ [A] | $I_{11}$ [A] | $I_{13}$ [A] | $THD_i\%$ | $THD_v\%$ |
|---|---|---|---|---|---|---|---|
| 0° | 319 | 68 | 23.08 | 14.45 | 7.17 | 23.16 | 9.4 |
| 30° | 279.5 | 75.65 | 23.95 | 10.2 | 10.14 | 30.6 | 8.9 |
| 45° | 238.2 | 75.8 | 21.86 | 5 | 8.35 | 36 | 8.4 |
| 60° | 166.95 | 69.45 | 27.7 | 21.3 | 10.66 | 47.87 | 10 |
| 75° | 92.45 | 53.55 | 35.95 | 9.5 | 13.78 | 73.6 | 8.9 |

Fig 4.19 shows the simulation results of the harmonic currents when varying the firing angle and $T_{load} = 100\%$.

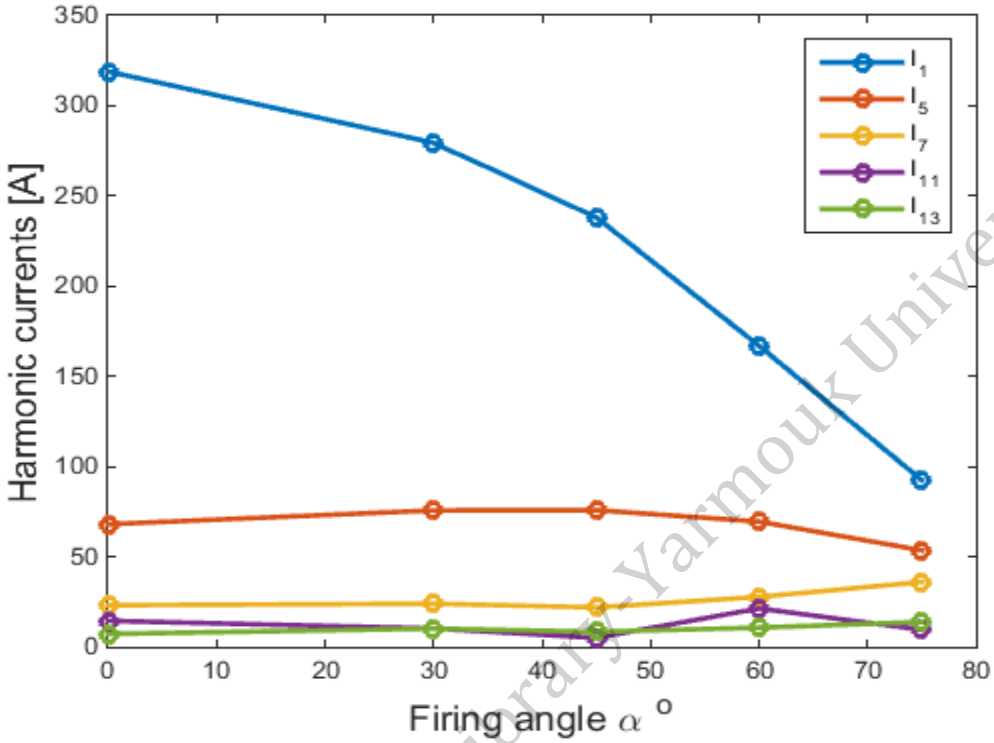


**Fig. 4.19** Simulated harmonic currents in terms of firing angle variation and $T_{load} = 100\%$.

Fig 4.20 shows the simulation results of the THDi for different load torque $T_{load}$ at various firing angle $\alpha$.

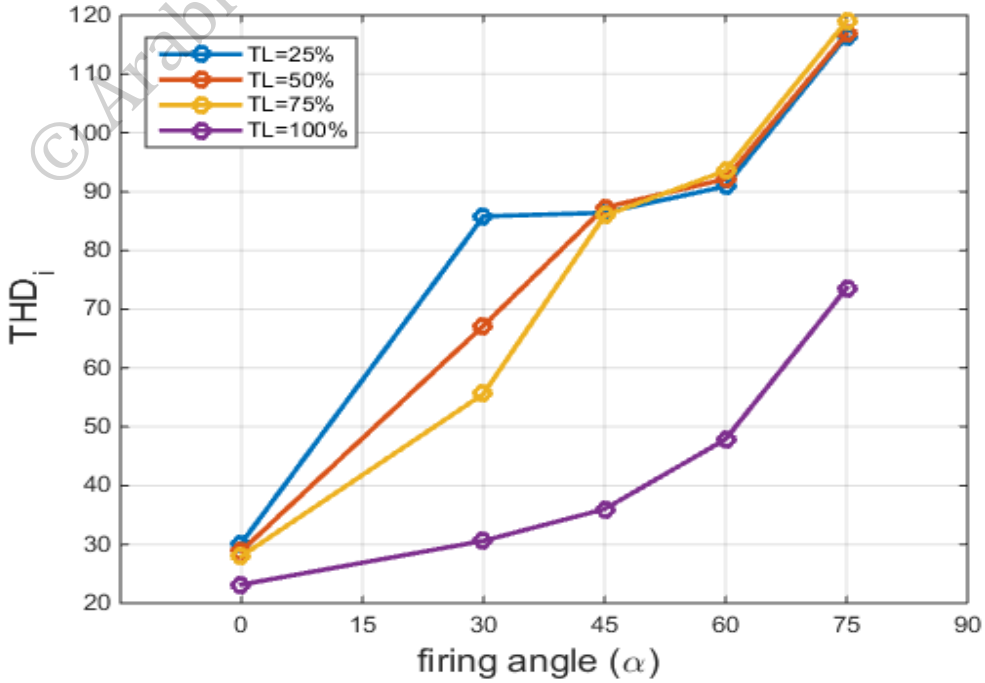


**Fig. 4.20** Firing angle Vs. Load Variation.

## 4.3 Harmonic Voltage Distortion Calculations

To determine whether harmonic distortion produced by the three phase controlled rectifier bridge driving a DC motor is acceptable or not then the THDv at PCC should be found. For instance, for case study 1 (Table 4.2), where the parameters are as follows:

$L_s = 0.18\,mH, R = 0.00567\,\Omega$, with additional AC inductance $L_{add} = 0.2\,mH$, without DC inductance $L_d$, the load torque $T_{Load}$=100% and firing angle $\alpha = 0$.

The harmonic voltages can be determined as in equation (4.6):

$$V_h = I_h * Z_h = I_h * [R + J\omega_1 h(L_s + L_{add})] \quad (4.6)$$

For $h = 5$, then $V_5 = I_5 * Z_5 = I_5 * [R + j\omega_1 * 5 * (L_s + L_{add})]$

$$= (52.9) * [0.00567 + j * 314 * 5 * (0.18 + 0.2) * 10^{-3}]$$

$$= 31.56\angle 89.2^{\circ}\ V$$

For $h = 7$, then $V_7 = I_7 * Z_7 = I_7 * [R + j\omega_1 * 7 * (L_s + L_{add})]$

$$= (17.2) * [0.00567 + j * 314 * 7 * (0.18 + 0.2) * 10^{-3}]$$

$$= 14.36\angle 89.6^{\circ}\ V$$

For $h = 11$ then $V_{11} = I_{11} * Z_{11} = I_{11} * [R + j\omega_1 * 11 * (L_s + L_{add})]$

$$= (7.4) * [0.00567 + j * 314 * 11 * (0.18 + 0.2) * 10^{-3}]$$

$$= 9.71\angle 89.75^{\circ}\ V$$

For $h = 13$, then $V_{13} = I_{13} * Z_{13} = I_{13} * [R + j\omega_1 * 13 * (L_s + L_{add})]$

$$= (3.5) * [0.00567 + j * 314 * 13 * (0.18 + 0.2) * 10^{-3}]$$

$$= 5.43\angle 89.79^{\circ}\ V$$

Where:

| | |
|---|---|
| $L_s$ | Source inductance. |
| $L_{add}$ | Additional inductance. |
| $\omega$ | The fundamental angular frequency. |

The THDv can be determined by equation (1.3):

$$THDv = \frac{\sqrt{31.56^2 + 14.36^2 + 9.71^2 + 5.43^2}}{\frac{460}{\sqrt{3}}} = 13.7\ \%$$

At PCC and when the bus voltage is equal to 69 KV and below (which is our case) the allowed THDv is only 5% or lower [3]. Since the resultant THDv is significantly high, other mitigation methods should be applied. For instance, single tuned passive filter can be tuned to cancel out specific harmonic order. It is not only characterized by low cost, but also it can provide power factor correction [31]. In the previous example, since the THDv is relatively high, this requires the use of multi single tuned filters in order to get lower voltage harmonic distortion. The highest harmonics ($5^{th}$, $7^{th}$, $11^{th}$, and $13^{th}$) can be eliminated; therefore, the parameters of each filter are determined.

To design single tuned passive filter to get rid of $5^{th}$ harmonic the following steps should be followed:

1. Decide the capacitor size $Q_c$ for the reactive power requirement of a harmonic source.
2. Calculate the reactance of the capacitor at fundamental frequency using $X_c = \frac{3V_{ph}^2}{Q_c}$.
3. Find the reactor that is necessary to tune the $h^{th}$ harmonic using $X_L = \frac{X_C}{h_{tuned}^2}$

   $Q_c$ can be calculated as in equation (4.7):

$$Q_c = P_L[\tan(\theta_{old}) - \tan(\theta_{new})] = \frac{3V_{ph}^2}{X_c} \qquad (4.7)$$

Let the new P.F =1.0 (unity power factor) $\Rightarrow\ \theta_{new} = 0^{\circ}$

and let the old P.F=0.9 $\Rightarrow\ \theta_{old} = 25.8^{\circ}$

$$Q_c = 200 * 746 * [\tan(25.8) - \tan(0)] = 72.12\ kVAR$$

The total $Q_c$ will be divided between two filters for the 5th and the 7th harmonic distortion:

From equation (4.7) $X_c$ is equal to:

$$X_c = \frac{3V_{ph}^2}{Q_c} = \frac{3 * 265^2}{\frac{72.1 * 10^3}{2}} = 5.84\ \Omega$$

$$X_c = \frac{1}{\omega_1 c} \Rightarrow c = \frac{1}{X_c \omega_1}$$

$$c_5 = \frac{1}{5.84 * 314} = 0.545\ mF$$

$$L_5 = \frac{X_c}{\omega_1 h^2} = \frac{5.84}{314 * 5^2} = 0.74\ mH$$

Similarly, $C_7$ and $L_7$ can be calculated:

$$C_5 = C_7 = 0.545\ mF$$

$$L_7 = \frac{X_c}{\omega_1 h^2} = \frac{5.84}{314 * 7^2} = 0.379\ mH$$

**Table 4.18** Filter parameters.

| **Undesired Harmonic Order** | **Filter Parameters** | |
|---|---|---|
| | ***L* [mH]** | **C [mF]** |
| **5th** | 0.74 | 0.545 |
| **7th** | 0.379 | 0.545 |

It is worth mentioning that the filter is usually tuned slightly lower than the intended harmonic order h. It is usually detuned to a lower frequency value of about $0.95h$. This detuning can prevent the harmonic component to be amplified due to the resonance that may arise after the single-tuned filter is installed [35].

Fig. 4.21 shows the THDv of case study 1 (Table 4.2), which is equal to 13.7 % and before adding the 5$^{th}$ and 7$^{th}$ single tuned passive filters:

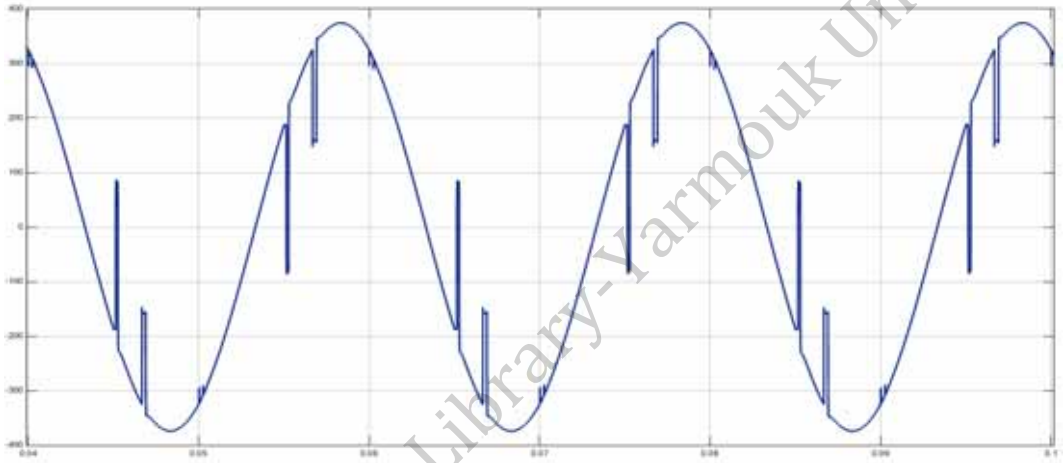

**Fig. 4.21** Voltage waveform of case study 1 before adding filters.

Fig. 4.22 shows the THDv of case study 1 (Table 4.2), which is equal to 4.8 % and after adding the 5$^{th}$ and 7$^{th}$ single tuned passive filters:

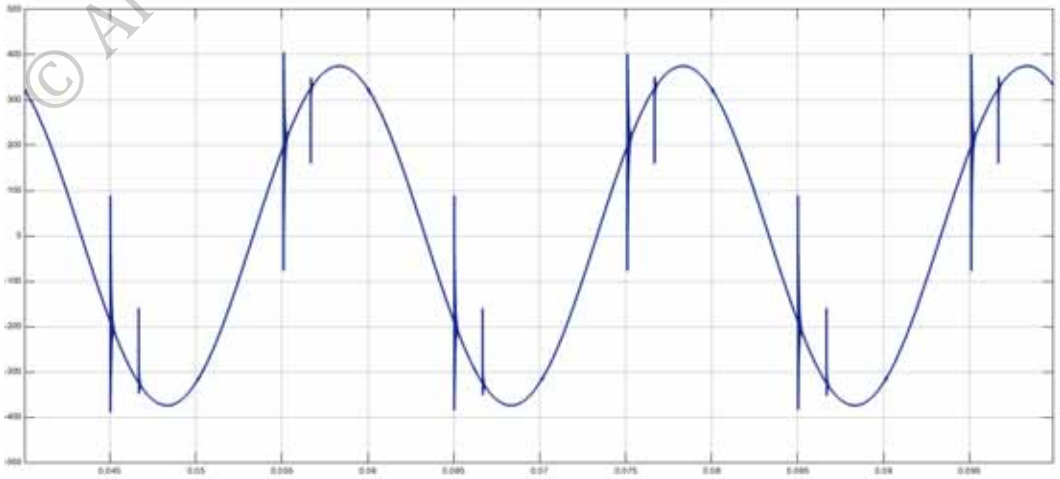

**Fig. 4.22** Voltage waveform of case study 1 after adding filters.

According to simulation results the THDv after adding the $5^{th}$ and $7^{th}$ single tuned passive filters is less distorted and is equal to 4.8%. This reduction in THDv is compatible with IEEE recommended standards [3].

Fig 4.23 to Fig 4.32 show the reduction effect of bigger values of $L_{add}$ over harmonic current waveform at different firing angle as well as the adverse effect of higher firing angles on THDi.

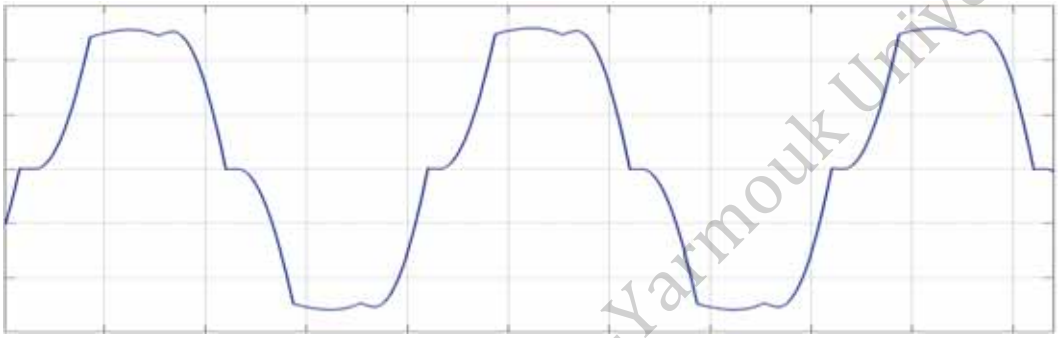

**Fig 4.23** Harmonic current waveform at firing angle$\alpha = 0^{\circ}$ and $L_{add} = 1.2\ mH$.

**Fig 4.24** Harmonic current waveform at firing angle$\alpha = 0^{\circ}$ and $L_{add} = 0.2\ mH$.

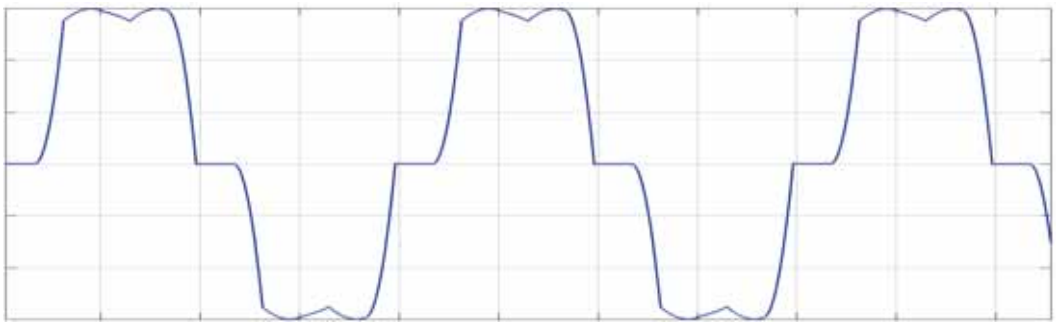

**Fig 4.25** Harmonic current waveform at firing angle$\alpha = 30^{\circ}$ and $L_{add} = 1.2\ mH$.

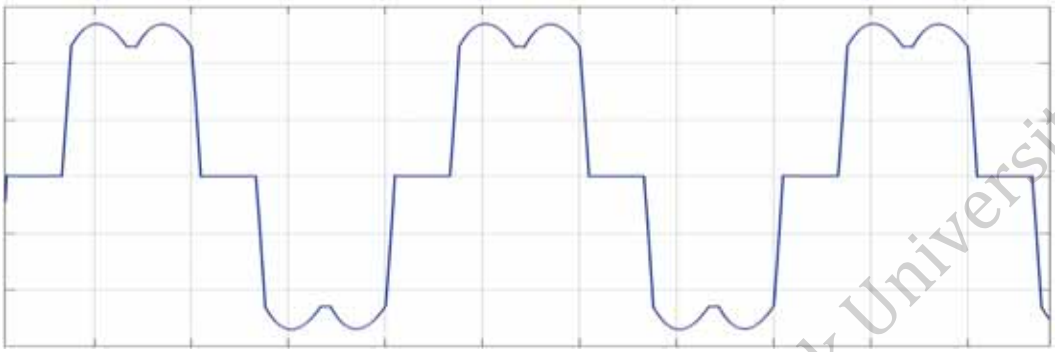

**Fig 4.26** Harmonic current waveform at firing angle$\alpha = 30^{\circ}$ and $L_{add} = 0.2\ mH$.

**Fig 4.27** Harmonic current waveform at firing angle$\alpha = 45^{\circ}$ and $L_{add} = 1.2\ mH$.

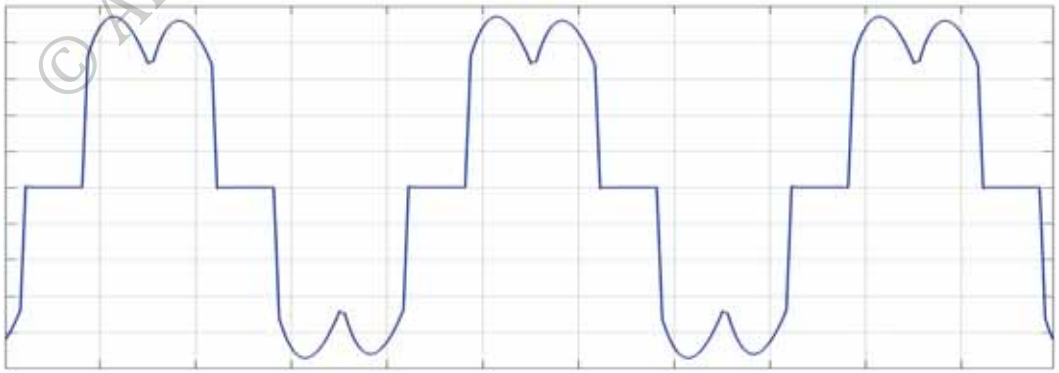

**Fig 4.28** Harmonic current waveform at firing angle$\alpha = 45^{\circ}$ and $L_{add} = 0.2\ mH$.

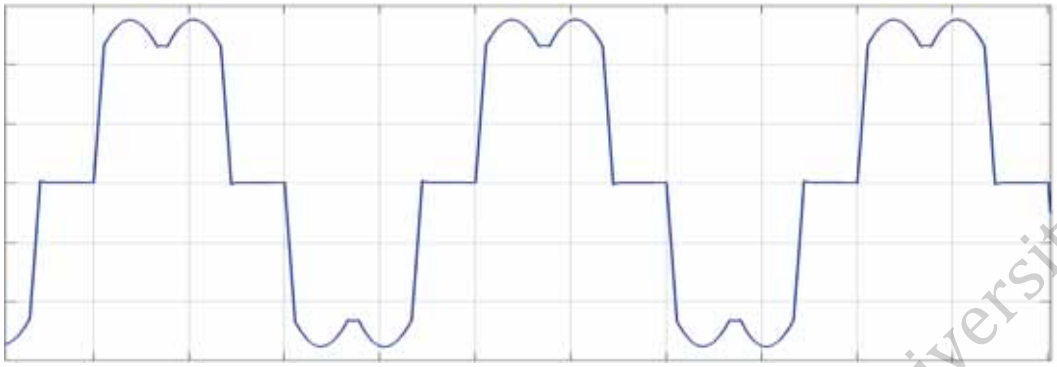

**Fig 4.29** Harmonic current waveform at firing angle$\alpha = 60^{\circ}$ and $L_{add} = 1.2\ mH$.

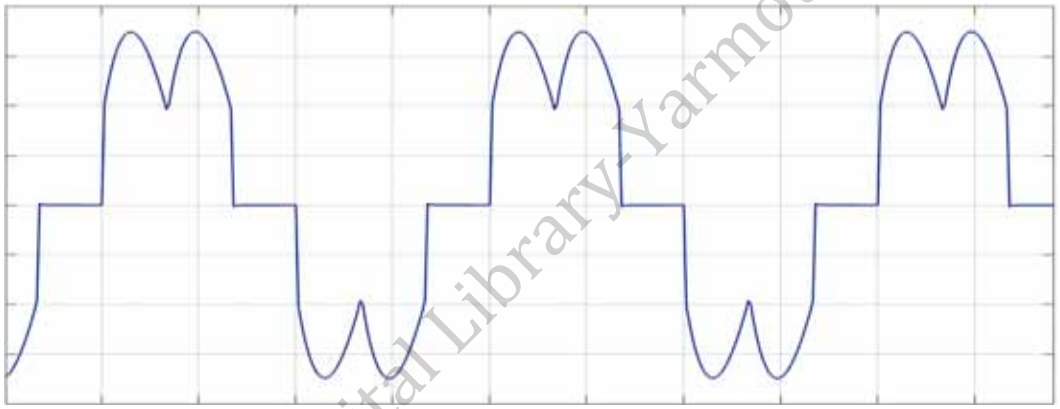

**Fig 4.30** Harmonic current waveform at firing angle$\alpha = 60^{\circ}$ and $L_{add} = 0.2\ mH$.

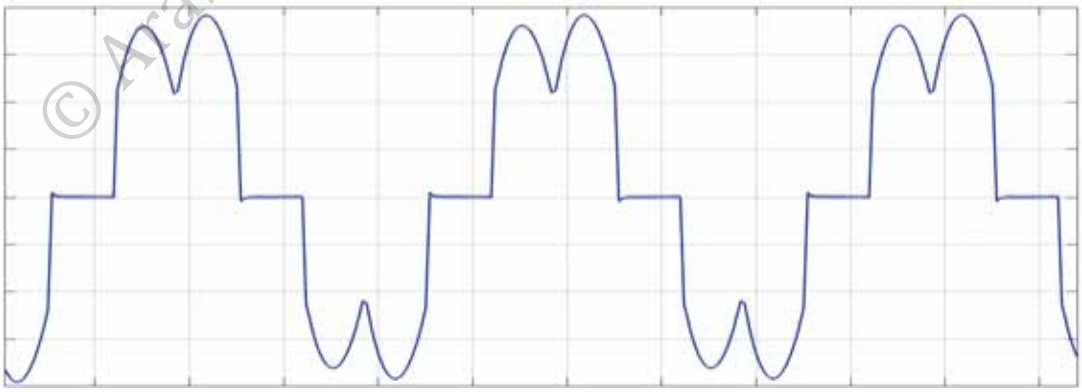

**Fig 4.31** Harmonic current waveform at firing angle $\alpha = 75^{\circ}$ and $L_{add} = 1.2\ mH$.

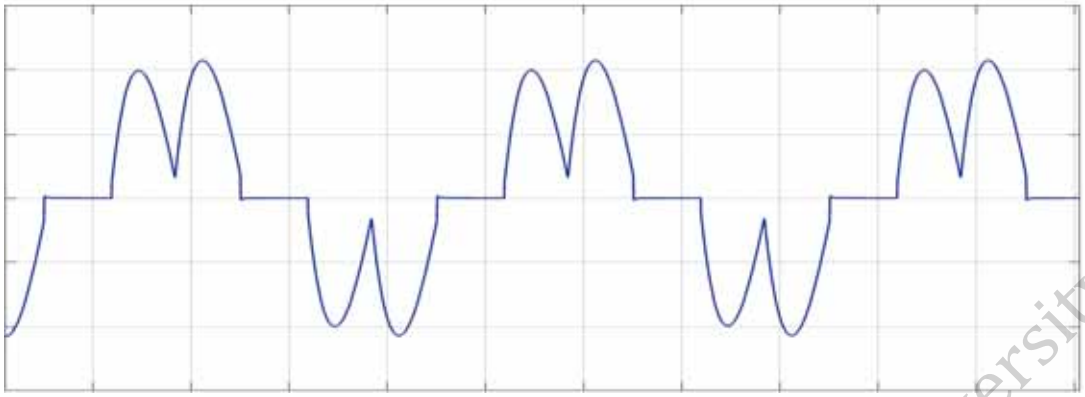

**Fig 4.32** Harmonic current waveform at firing angle $\alpha = 75^{\circ}$ and $L_{add} = 0.2\ mH$.

It can be concluded from the simulation results that under the same loading condition and the same firing angle the $L_{add}$ has higher harmonic reduction effect at the ASD input compared to $L_d$ effect. For instance, when $L_d$ is equal to 1 mH the THDi will result in the same percentage of the THDi when $L_{add} = 0.6$ mH. Moreover, higher THDi will result when using higher firing angle for all different cases. Additionally, in terms of firing angle variations versus different load percentage, the simulation results show that the amount of current distortion is at its minimum when operating at lower firing angle and higher load percentage. It is noted that THDi differences between curves do not change by equal distances for each equal increment of Ladd or Ld. Thus, it can be concluded that there is a limit for THDi mitigation through addition of passive elements regardless of the firing angle.

# CHAPTER FIVE:

## Conclusion and Future Work

# Chapter Five Conclusion and Future Work

## 5.1. Conclusion

In this work, the performance of a practical 6-pulse bridge rectifier driving a separately excited DC motor is investigated. Evaluation of the line-side harmonic currents in terms of firing angle variation is conducted and simulated using MATLAB software. The system parameters are varied, and the corresponding THDv and THDi are calculated for each study. It is known that additional AC inductance $L_{add}$ and/or DC link inductance $L_d$ are used to reduce the amount of line side harmonics and which results in THDi reduction. However, the simulation results show that increasing $L_{add}$ and/or $L_d$ above certain values will not have significant effect on harmonic currents and THDi. Therefore, there are certain limits govern such approach. As a result, alternative mitigation techniques should be applied when less distortion is needed such as active or passive filters. The ultimate way to get rid of harmonic currents produced by a single ASD is to use $L_{add}$ and/or $L_d$ without the need to use other filtering types. Nevertheless, when the electrical power system includes large amount of THDi, in this case it is easier to use passive or active filters. Simulation results show a good reduction effect when adding the $5^{th}$ and the $7^{th}$ single tuned passive filters to the system under study. For case study 1, the THDv was about 13.7 % before inserting the filter. However after adding the $5^{th}$ and the $7^{th}$ harmonic filter, the THDv has reduced to 4.8 % which is in compliance with IEEE standard 1992. The reason which led to increase of THDi with increasing firing angle can be explained logically by the fact that, the thyristor is turned on with a delay angle $\alpha$ therefore, distorted line current will arise, that means the more delay angle the more the value of THDi will be.

## 5.2. Future Work

In this thesis, the line side harmonics produce by fully-controlled 6-pulse bridge rectifier in terms of firing angle variation is assessed.

For a future work, investigating the usage of active filter instead of passive filters, because passive filters may case resonance in the system. Extended the work for 12-pulse, 18-pulse or higher pulse order. Investigating practical system taking into consideration power system line impedance.

## References


[1] A. Chikh, A. Chandra, "Optimization and control of a photovoltaic powered water pumping system," *Electrical Power & Energy Conference (EPEC)*, 2009, pp. 22-23.

[2] R. C. Dugan and others, *Electrical Power Systems Quality*, 3rd Edition. McGraw-Hill Professional, 2012, pp.15-67.

[3] IEEE Recommended Practice and Requirements for Harmonic Control in Electric Power Systems," *IEEE Standards 519-1992*, pp.1-29, June 11 1992.

[4] K.N. Sakthivel, S.K. Das and K.R. Kini, "Importance of quality AC power distribution and understanding of EMC standards IEC 61000-3-2, IEC 61000-3-3 and IEC 61000-3-11," *Electromagnetic Interference and Compatibility, 8th International Conference*, pp.423,430, 18-19 Dec. 2003.

[5] M. H. Bollen, *Understanding power quality problems,* Series Editor, New York, 2000.

[6] M. T. Bishop, A.V. Do and S. R. Mendis, "Voltage flicker measurement and analysis system," *IEEE Computer Application in Power,* vol. 7, no.4, pp. 650-655. 1994.

[7] F.Z. Peng, "Harmonic sources and filtering approaches," *IEEE Ind. Appl. Mag.*, vol.7, no.4, pp.18-25, Jul/Aug 2001.

[8] T.E. Grebe, "Application of distribution system capacitor banks and their impact on power quality," *IEEE Trans. Ind. Appl.*, Vol. 32, Issue 3, May/Jun 1996.

[9] D. Said, K. Nor, "Effects of harmonics on distribution transformers," *Power Engineering Conf, Australasian Universities*, 14-17 Dec. 2008, pp.1-5

[10] D. Yildirim and E.F. Fuchs, "Measured transformer derating and comparison with harmonic loss factor ($F_{HL}$) approach," *IEEE Trans. Power Del.*, vol.15, no.1, pp.186-191, Jan 2000.

[11] A. Domijan and E. Embriz-Santander, "Harmonic mitigation techniques for the improvement of power quality of adjustable speed drives (ASDs)" Applied Power Electronics Conf and Expo. 1990. pp.96-105.

[12] A. Hussein Kazem, A. A. Alblushi, S. Ali. Aljabri and H. Khmais Alsaidi, "Simple and Advanced Models for Calculating Single-Phase Diode

Rectifier Line-Side Harmonics", *IEEE Trans. Ind. Appl*., Vol.9, pp. 179-183, November 2005.

[13] S. Hansen, L. Asiminoaei and F. Blaabjerg, "Simple and advanced methods for calculating six-pulse diode rectifier line-side harmonics," *in Proceedings. 38th annual. IEEE conference.* 2003, pp.2056-2062.

[14] L. Asiminoaei, F. Blaabjerg and S. Hansen, "Harmonic calculation toolbox in industry application for adjustable speed drive," *in Proc. 19th annual. IEEE APEC conference*, 2004, pp.1628-1634.

[15] L. Asiminoaei, S. Hansen and F. Blaabjerg, "Harmonic calculation software for industrial applications with adjustable speed drives," *Power Electronics and Applications, European Conf*erence., 2005, P.10.

[16] L. Asiminoaei, S. Hansen and F. Blaabjerg, "Development of calculation toolbox for harmonic estimation on multi-pulse drives," in Proc. 39th Annual. *Industry Applications Conference*., pp.878-885.

[17] Z. A. Ali Akbar and M. Birjandi, (2012, May). Three Phase Controlled Rectifier Study in Terms of firing angle variations [Online]. Available: http://www.slideshare.net.

[18] J. Schaefer. *Rectifier Circuits Theory and Design*, Wiley, 1965, pp-104-116.

[19] J.C. Read, "The calculation of rectifier and inverter performance characteristics," Electrical Engineers - Part II: Power Engineering, Journal of the Institution of vol.92, no.29, pp.495-509, October 1945.

[20] A. Graham, D. Schonholzer, and Emil T, "Line Harmonics of Converters with DC-Motor Loads," *IEEE Trans. Industry Appl.*, vol.19, no.1, pp.84-93, Jan. 1983.

[21] J. Mcfarlane and M. J. Harris, "The control of Flux Waveforms in Iron Testing by the Application of Feedback Amplifier Techniques," *in Proceed. IEE-Part A: Power Engineering*, vol. 104, 1958, pp.395-402.

[22] H. Sasaki, T. Machida, "A New Method to Eliminate AC Harmonic Currents by Magnetic Flux Compensation-Considerations on Basic Design," *IEEE Trans. Syst*., vol. 90, no. 5, pp. 209-211, 1971.

[23] H. Akagi, E. H. Watanabe and M. Aredes, Instantaneous Power Theory and Applications to Power Conditioning, Hoboken, NJ: John Wiley & Sons, Inc., 2007.

[24] A. Zobaa, *power quality issues,* 1st Edition, InTech, 2013, pp. 105-135.

[25] S. Pyakuryal and M. Matin, "Implementation of AC to DC converter using Thyristor on ATP", *IOSR Journal of Engineering*, Vol. 2, no. 11, pp. 6-11, Nov 2012.

[26] S. Pyakuryal and M. Matin, "Harmonic Analysis for a 6-pulse Rectifier", *IOSR Journal of Engineering*, Vol. 3, no. 3, pp. 57-60, March 2013.

[27] B. Wu, *High Power Converters and AC Drives*, 1st Edition. Wiley, 2006, pp.65-80.

[28] N. Mohan, T. Undeland, and W. P. Robbins, *Power Electronics: Converters, Applications, and Design*, 2nd Edition, Hoboken, NJ: John Wiley & Sons, 1995.

[29] X. Liang, O. Ilochonwu and, J. Lim, "Influence of reactors on input harmonics of variable frequency drives," *Industrial and Commercial Power Systems Technical Conference*, pp. 1-9, 15 May 2011.

[30] http://www.mathworks.com/help/physmod/sps/powersys/ug/simulating-a-dc-motor-drive.html

[31] J.C. Das, "Passive filters - potentialities and limitations," *IEEE Trans. Ind. Appl.*, vol.40, no.1, pp.232- 241, Jan.-Feb. 2004.

[32] S. Yousif, M. Wanik, A. Mohamed, "Implementation of different passive filter designs for harmonic mitigation," *Power and Energy Conference*., 29-30 Nov. 2004, pp.229-234.

[33] H. Wu, Y. Chang, Y. Feng, "A novel active power filter for harmonic suppression," *IEEE Trans. Power Del*., vol.20, no.2, April 2005, pp.1507-1513.

[34] L. Moran, L. Fernandes, J. Dixon and R. Wallace, "A simple and low cost control strategy for active power filters connected in cascade," *IEEE Transaction on Industrial Electronics*, vol. 44, Oct. 1997, pp. 621-629.

[35] J. Arrillaga and N.R. Watson, Power Systems Harmonic, 2nd ed, New York: Wiley, 2003.

**الاسم :** محمد نبراس محمد فاروق أبوالشامات

**عنوان الرسالة :** تقصي التوافقيات في طرف التغذية و الناتجة عن مقوم ثلاثي الطور بدلالة تغيرات زاوية القدح.

**الدرجة :** الماجستير في العلوم.

**الجامعة :** اليرموك.

**المشرف :** الاستاذ الدكتور محمد بشير الرفاعي.

**التاريخ :** ٢٠١٥/٨/١٠

**الملخص التجريدي**

يعتبر جسر التقويم ثلاثي الطور المقاد ذو الستة نبضات أحد أهّم التطبيقات المستخدمة للتحكم بسرعة المحركات الكهربائية و ذلك لسعره المنخفض و كفاءته العالية. لكن في المقابل يعبر أحد أكثر التطبيقات توليدا للتوافقيات على جانب خط النقل ذو التردد المتناوب. وللحد من الأثار السلبية الناتجة عن إستخدام مثل هكذا تطبيق مثل زيادة مفاقيد وحرارة الآلات الكهربائية، يقوم مشغلو نظم القدرة الكهربائية بدراسة مستويات هذه التوافقيات و اقتراح الحلول المناسبة للتخفيف منها.

يقوم هذا البحث بتقصي مدى تأثير تغيير زاوية القدح على مستوى التوافقيات المتولدة من جهة خط النقل ذو التردد المتناوب وذلك عند إستخدام محرك تيار مستمر ذو تهيج مستقل مقاد من قبل مقّوم ثلاثي الطور، بالإضافة إلى دراسة مدى تأثير تغيّر بارمترات (معطيات) هذه الدارة على مستويات التوافقيات.

في البداية، تم إستخدام برنامج الماتلاب لنمذجة محرك التيار المستمر ذو التهيج المستقل و جسر التقويم ثلاثي الطور المقاد، أخذين بعين الإعتبار ممانعة خطوط النقل المغذية لهذا المقوم، و من ثم تم دراسةً تغيّر كلا من زاوية القدح، قيمة الحمل، مفاعلة خط النقل (Line-reactor) بالإضافة إلى خانق الترابط المستمر (DC-link Choke) على مستويات التوافقيات المتولدة من جهة خط النقل.

أخيرا، تم تقديم البيانات و الجداول المتعلقة بتحديد قيم التيارات التوافقية و مستوى التشوه الكلي للتيار من جهة خط النقل وذلك عند تغيّر زاوية القدح.

**الكلمات المفتاحية:** جسر تقويم ثلاثي الطور المقاد، مستوى التشوه الكلي للتيار، التوافقيات، مفاعلة خط النقل، خانق ترابط مستمر.

# APPENDIX

## Matlab Codes

**Six Pulse Practical Rectifier Bridge parameters code**

```
clear all
close all
clc

TL = 815;
Ls = 0.2e-3;
firing_Angle = 45;
Ld = 0.2e-3;
Psc = 25 * 200 * 746;
Vll = 460;
f= 50;
w= 2*pi*f;
Z = Vll.^2/Psc;
ratio = 10;
R = Z/ratio;
L = Z / w ;
sim('sixpulse')
```

**Six Pulse Ideal Bridge Rectifier plots code**

```
clear all
close all
clc

R_load= 5;
L_load= 10e-3;
Ls = 0;
firing_Angle = 30;
Ld = 0;
sim('sixpulseIdeal')

%% save data from simulink model
vax=va;
vbx=vb;
vcx=vc;
vpx=vp;
vnx=vn;
vox=vo;
iax=ia;
ibx=ib;
icx=ic;
p1x=p1;
p2x=p2;
p3x=p3;
p4x=p4;
p5x=p5;
p6x=p6;

%% choose part of signals
```

```
div=21;
xmin=2500;
xmax=8500;
datamin = 1;
datamax = 50000;

va=vax(datamin:datamax);
vb=vbx(datamin:datamax);
vc=vcx(datamin:datamax);
vp=vpx(datamin:datamax);
vn=vnx(datamin:datamax);
vo=vox(datamin:datamax);
ia=iax(datamin:datamax);
ib=ibx(datamin:datamax);
ic=icx(datamin:datamax);

%% plot Vin
figure(1)
subplot(div,1,[1 2 3])
hold on
plot(va,'b','linewidth',2)
plot(vb,'r','linewidth',2)
plot(vc,'g','linewidth',2)
xlim([xmin xmax])
set(gca,'xtick',[])
set(gca,'ytick',[])
ylabel('V','fontsize',14)

%%  plot pulse signals

subplot(div,1,4)
plot(p3(1:5:end),'k','linewidth',2)
xlim([xmin xmax])
set(gca,'xtick',[])
set(gca,'ytick',[])
ylabel('P1','fontsize',10)

subplot(div,1,5)
plot(p5(1:5:end),'k','linewidth',2)
xlim([xmin xmax])
set(gca,'xtick',[])
set(gca,'ytick',[])
ylabel('P2','fontsize',10)

subplot(div,1,6)

plot(p1(1:5:end),'k','linewidth',2)
xlim([xmin xmax])
set(gca,'xtick',[])
set(gca,'ytick',[])
ylabel('P3','fontsize',10)

subplot(div,1,7)
plot(p6(1:5:end),'k','linewidth',2)
xlim([xmin xmax])
```

```
set(gca,'xtick',[])
set(gca,'ytick',[])
ylabel('P4','fontsize',10)

subplot(div,1,8)
plot(p2(1:5:end),'k','linewidth',2)
xlim([xmin xmax])
set(gca,'xtick',[])
set(gca,'ytick',[])
ylabel('P5','fontsize',10)

subplot(div,1,9)
plot(p4(1:5:end),'k','linewidth',2)
xlim([xmin xmax])
set(gca,'xtick',[])
set(gca,'ytick',[])
ylabel('P6','fontsize',10)

%% plot Vp & Vn

subplot(div,1,[10 11 12])
cla
hold on
plot(vp,'k','linewidth',2)
plot(vn,'k','linewidth',2)
xlim([xmin xmax])
set(gca,'xtick',[])
set(gca,'ytick',[])
ylabel('V','fontsize',14)

%% plot Vo
subplot(div,1,[13 14 15])
plot(vo,'b','linewidth',2)
xlim([xmin xmax])
set(gca,'xtick',[])
set(gca,'ytick',[])
ylabel('Vo','fontsize',14)

%% plot currents

subplot(div,1,[16 17])
plot(ic,'b','linewidth',2)
xlim([xmin xmax])
set(gca,'xtick',[])
set(gca,'ytick',[])
ylabel('ia','fontsize',14)
ylim([min(ic)-5 max(ic)+5])

subplot(div,1,[18 19])
plot(ia,'r','linewidth',2)
xlim([xmin xmax])
set(gca,'xtick',[])
set(gca,'ytick',[])
ylabel('ib','fontsize',14)
ylim([min(ia)-5 max(ia)+5])
```

```
subplot(div,1,[20 21])
plot(ib,'g','linewidth',2)
xlim([xmin xmax])
set(gca,'xtick',[])
set(gca,'ytick',[])
ylabel('ic','fontsize',14)
ylim([min(ib)-5 max(ib)+5])
```

**THDi Vs firing angles plots code**

```
clear all
close all
clc

%% Case 1
data = xlsread('data1.xlsx','Case1')
data = fliplr(data);
THDi = data(:,end);
data(:,end)=[];
THDi = reshape(THDi,5,6)
firing_angle = [0 30 45 60 75 ];
figure(1)
plot(firing_angle,THDi,'-o','linewidth',2)
xlabel('firing angle (\alpha) ' ,'fontsize',14  )
ylabel('THD_i' ,'fontsize',14 )
set(gca,'xtick',[0 15 30 45 60 75 90])
xlim([-15 90])
grid on
legend('L_a_d_d = 0.2mH','L_a_d_d = 0.4mH','L_a_d_d =
0.6mH','L_a_d_d = 0.8mH','L_a_d_d = 1.0mH','L_a_d_d =
1.2mH','location','NW')

%% Case 2
data = xlsread('data1.xlsx','Case2')
data = fliplr(data);
THDi = data(:,end);
data(:,end)=[];
THDi = reshape(THDi,5,6)
firing_angle = [0 30 45 60 75 ];
figure(2)
plot(firing_angle,THDi,'-o','linewidth',2)
xlabel('firing angle (\alpha) ' ,'fontsize',14  )
ylabel('THD_i' ,'fontsize',14 )
set(gca,'xtick',[0 15 30 45 60 75 90])
xlim([-15 90])
grid on
legend('L_d = 0.2mH','L_d = 0.4mH','L_d = 0.6mH','L_d =
0.8mH','L_d = 1.0mH','L_d = 1.2mH','location','NW')

%% Case 3
data = xlsread('data1.xlsx','Case3')
data = fliplr(data);
THDi = data(:,end);
data(:,end)=[];
```

```
THDi = reshape(THDi,5,4)
firing_angle = [0 30 45 60 75 ];
figure(3)
plot(firing_angle,THDi,'-o','linewidth',2)
xlabel('firing angle (\alpha) ' ,'fontsize',14  )
ylabel('THD_i' ,'fontsize',14 )
set(gca,'xtick',[0 15 30 45 60 75 90])
xlim([-15 90])
grid on
legend('TL=25%','TL=50%','TL=75%','TL=100%','location','NW')
```